

THE VERTICAL STRUCTURE AND STABILITY OF ALPHA MODEL ACCRETION DISKS

J. K. CANNIZZO AND J. C. WHEELER
 Department of Astronomy, University of Texas at Austin
 Received 1983 July 22; accepted 1983 December 15

ABSTRACT

A limit cycle driven by thermal instabilities in the accretion disk may account for the periodic outbursts of cataclysmic variables and certain X-ray transients. The outbursts will depend on specific properties of the vertical accretion disk structure such as convection, partial ionization, opacity, and viscosity. As a step toward understanding the physical processes that determine the time-dependent nature of accretion disks, we have undertaken a parameter study of the vertically explicit structure corresponding to steady-state, α -model, thin-disk accretion for accreting objects of $1 M_{\odot}$. Solutions are presented for $10^9 \leq r(\text{cm}) \leq 10^{11}$; $10^{-14} \leq \dot{M}(M_{\odot}\text{yr}^{-1}) \leq 10^{-7}$; $10^{-4} \leq \alpha \leq 1.0$. Particular attention is paid to the role of convection in the vertical structure and to the location of critical points which represent the onset of thermal instability. Optically thin conditions are also examined in detail. The presence of molecules at low temperatures gives rise to double-valued, discontinuous solutions separated by “forbidden” regions. We show that the temperature in quiescence is likely to be low ($T < 2500$ K) for the bulk of the matter. Quiescent temperatures of ~ 6000 K are possible in thermal equilibrium only for $r < 7 \times 10^9$ cm for $\alpha = 0.1$. This will promote the storage of material in an outer, cold ring. Scaling laws are presented for the fundamental properties of the vertically explicit models, and these are used to derive time scales for various idealized phenomena. We present an ordering of three disk time scales. This ordering would enable one to discriminate between different models were realistic characterizations of the time scales available. We compare the instability associated with hydrogen recombination with the instability associated only with the onset of convection.

Subject headings: stars: accretion — stars: binaries — stars: dwarf novae — X-rays: bursts

I. INTRODUCTION

Mass transferred onto a compact companion in a binary system has a preferred sense of angular momentum and is thought to form a geometrically thin disk. Any viscosity will subsequently cause this material to spiral to smaller radii. The study of accretion disks has matured in the last decade (Pringle 1981) but is still hampered by a lack of understanding of the physical nature of the viscosity. Time-dependent accretion phenomena provide a means by which empirical bounds can be put on the viscosity, but the cause of the time dependence is generally ill-understood, so the issues of viscosity and time dependence are coupled in a confusing manner.

Although much attention has been focused on accretion disks by the revelations from X-ray astronomy concerning binary neutron star systems, the best laboratory for testing accretion disk theory probably remains the classical cataclysmic variables (Robinson 1976). In these systems a star, normally a main-sequence dwarf, fills its Roche lobe and transfers mass onto a white dwarf. These systems can be studied at optical wavelengths where the disk may produce the bulk of the flux. Classical novae, aside from their rare thermonuclear outbursts, appear to accrete steadily at relatively high mass transfer rates, in excess of $\sim 10^{-9} M_{\odot} \text{ yr}^{-1}$ (Smak 1982*b*, 1983*a*). A long-standing problem is the origin of the

outbursts of the dwarf novae for which the transfer rate is smaller. Dwarf novae erupt on time scales of months, producing an outburst lasting a week or so. Even without a fundamental understanding of the nature of the dwarf nova instability, these outbursts set some constraints on the viscosity. Observed decay times of dwarf nova outbursts show the viscosity coefficient in the disk to be of order $10^{15} \text{ cm}^2 \text{ s}^{-1}$ (Mantle and Bath 1983), much larger than molecular viscosities which are of order $1 \text{ cm}^2 \text{ s}^{-1}$. Hence, some additional viscosity, usually postulated to be turbulent or magnetic, must exist. Progress toward understanding the dwarf nova outbursts thus promises to lead to a more fundamental understanding of the viscosity in general.

A popular hypothesis to account for the outbursts of dwarf novae has been that material is stored in an outer ring and then suddenly accreted onto the white dwarf (Osaki 1974; Smak 1971, 1976; Hoshi 1979, 1981, 1982). The problem with this hypothesis has been the lack of any realistic physical basis. Several independent groups of investigators have recently realized that the key to understanding dwarf nova outbursts and related phenomena may be the study of accretion disks using realistic input physics to construct detailed models of the vertical structure. Such structure can naturally lead to thermal instabilities. The interplay of viscous heating with temperature-sensitive cooling resulting from diffusion or

convection can produce double-valued temperature solutions for a given disk surface density and transitions between these alternate states, depending on whether the heating or cooling dominates. The possibility is raised that matter will build up in a cooler, low-viscosity state and then undergo a spontaneous transition to a hotter, high-viscosity state.

Cannizzo (1981) explored the double-valued nature of vertical disk structure induced by partial ionization in the context of disks around supermassive black holes. Meyer and Meyer-Hofmeister (1981, 1982; hereafter MM1 and MM2, respectively), first presented the possibility of a limit cycle behavior in dwarf novae resulting from similar effects in the stellar case. Smak (1982*a*, *b*, 1983*a*, *b*) has also constructed models for disks in cataclysmic variable systems with detailed vertical structure and discussed the effect of such structure on the stability of the accretion flow. Cannizzo, Ghosh, and Wheeler (1982; hereafter CGW) presented vertically explicit models of stellar accretion disks including optically thin portions and pointed out the thermal nature of the instability implicit in the structure for temperatures associated with hydrogen recombination. They showed that another thermal instability would be induced at lower temperatures, ~ 2000 K, if the outbreak of midplane convection resulted in an increase in viscosity compared to radiative regions with similar conditions of density and temperature. They argued that the instability associated with hydrogen recombination would tend to lead to outbursts beginning at small radii where little mass was stored and, hence, in bursts which were too frequent and of too low luminosity to correspond to observed dwarf novae. The low-temperature instability seemed to provide a better match to observations. If confirmed, this would provide another partial, if crude, constraint on the viscosity of accretion disk matter. Cannizzo, Wheeler, and Ghosh (1982, 1983) extended the argument that the low-temperature instability better reproduced the observations. They pointed out that a smaller viscosity parameter in cold radiative regions may be physically plausible. Such regions will be devoid of turbulence associated with convection, and the partial ionization will be so low that magnetic flux will not be frozen in the gas, precluding an efficient dynamo. They presented preliminary results of time-dependent models of the resulting outburst which displayed recurrence times, luminosities, and decay times in reasonable accord with dwarf novae. They also discussed the application of the theory to certain types of X-ray transients. Faulkner, Lin, and Papaloizou (1983; hereafter FLP), Papaloizou, Faulkner, and Lin (1983; hereafter PFL), Smak (1983*a*), Mineshige and Osaki (1983), and Meyer and Meyer-Hofmeister (1984; hereafter MM4) have explored the vertical structure and have begun to address the complex question of the global response of the disk to repeated instabilities in the context of nonthermal equilibrium evolution.

In §§ II and III of this paper we concentrate on understanding the physics that determines the steady-state vertical structure of accretion disks for a wide range of conditions. We discuss the comparison of our results to those of other workers in some detail. The implications of our steady-state calculations for time-dependent situations are explored and we give a brief discussion of observations in § IV, and our conclusions are summarized in § V.

II. STEADY-STATE DISK THEORY

a) Alpha Model Disks

The general equations governing steady-state disk structure are the following:

Viscous (shear) energy generation:

$$\epsilon = t_{\phi r}(-r d\Omega/dr), \quad (1)$$

Hydrostatic equilibrium:

$$\nabla P = -\rho \mathbf{g}, \quad (2)$$

Energy transport:

$$\begin{aligned} F = & -4/3 ac/\kappa\rho T^3 \nabla T \\ & + c_p \rho (g/T)^{1/2} l^2/4 (|\nabla T| - |\nabla T_{\text{ad}}|)^{3/2} \hat{\mathbf{n}}, \end{aligned} \quad (3)$$

where all symbols have their standard meanings and $\hat{\mathbf{n}}$ is the unit direction vector of the convective flux.

One approach to geometrically thin disk accretion is the α -theory of Shakura and Sunyaev (1973; hereafter SS). In this approach the viscous stress tensor is set equal to an unknown constant $\alpha \leq 1$ times the pressure. SS solved for the disk structure by neglecting convection and invoking a vertical averaging procedure in which the gradient ∇ is replaced by $1/h$, where h is the disk semithickness. This reduces the above differential equations to algebraic equations. The structure equations then become

$$F/h = 3/2 \alpha \Omega P, \quad (4)$$

$$P/h = \rho \Omega^2 h, \quad (5)$$

and

$$F = 4/3 ac/\kappa\rho T^4/h. \quad (6)$$

One can also derive an equation relating energy flux to accretion rate. It is

$$F_s = 3/8\pi \dot{M} \Omega^2 \left[1 - \beta \sqrt{r_{\text{wd}}/r} \right], \quad (7)$$

where r_{wd} is the radius of the white dwarf and β is a parameter measuring the flux of angular momentum across r_{wd} (Novikov and Thorne 1973). These equations can then be solved algebraically for a given equation of state and opacity. SS presented analytic solutions for three regions: (i) $P = P_r$, $\kappa = \kappa_{\text{es}}$; (ii) $P = P_g$, $\kappa = \kappa_{\text{es}}$; and (iii) $P = P_g$, $\kappa = \kappa_0 \rho T^{-7/2}$. A numerical integration of equations (1)–(3) over the vertical structure using realistic opacities and thermodynamic parameters produces solutions which agree well with these “vertically averaged” results if the solutions are free of convection. In particular, we find that midplane temperatures and surface densities agree to within $\sim 20\%$ – 30% for given r , \dot{M} , and α if accurate coefficients for mean molecular weight μ and Rosseland opacity κ are used in the solutions given by SS.

b) Convection

The assumption of pure radiative diffusion can lead to a seriously erroneous solution if $\nabla > \nabla_{\text{ad}}$ somewhere in the vertical structure. Suppose such a solution showed only a thin strip near the disk surface which was convectively unstable, as shown schematically in Figure 1a. If one then introduced convection in the unstable region, the temperature gradient in this strip would be decreased. In the steady state with energy transport only in the vertical direction, the mass accretion rate determines the flux at a given radius (see SS) and hence the effective temperature in the one-dimensional geometry. The temperature gradient can be reduced in the convectively unstable region only at the expense of inducing a superadiabatic temperature gradient in a deeper region which was originally convectively stable, as shown in Figure 1b. A fully consistent solution may turn out to be completely convective as in Figure 1c. We and others find that precisely this extreme situation arises for solutions with convection induced by the "opacity peak" (see § IIIbiii). Pure radiative solutions show only a thin convectively unstable strip near the surface, whereas solutions with radiative transport *and* convection give solutions with convection extending from midplane to surface, and midplane temperatures much smaller than those given by the purely radiative solutions. This is in contrast to stars where the extreme sensitivity of nuclear reaction rates to temperature tends to yield a fixed central temperature. The inclusion of convection in an outer superadiabatic region (Fig. 1d) does not disturb the inner structure set by the nuclear burning but results only in a small change in the effective temperature (Fig. 1e) which can be accommodated at constant luminosity in the two-dimensional geometry by a change in radius.

Taylor (1980) derived inequalities giving necessary conditions for convection to occur in disks with power-law expressions for opacity and viscosity. For gas pressure-dominated α -disks with $\kappa = \kappa_0 \rho^a T^b$ the necessary condition for convective instability is $3a + 2b > -2$. For $a = 0$ or 1, the critical value for neutral stability is $b_{\text{crit}} = -1$ or -2.5 , respectively. Hence, Taylor predicts that solutions with Kramers's like opacity ($a \approx 1, b \approx -3.5$) should not be convectively unstable, which we find to be the case. However, as T decreases and approaches 10^4 K, b becomes less negative and then becomes positive and large as the peak in Rosseland opacity is passed. Solutions with $T = 10^4$ K somewhere in their vertical structure are found to be convective just as are the layers of partial ionization in stars.

Several investigators have constructed vertically explicit thin disk solutions for various assumptions concerning viscosity, opacity, and equation of state (Koen 1976; Vila 1978, 1980; Kozłowski, Wiita, and Paczyński 1979; Lin and Papaloizou 1980; Cannizzo 1981; Robertson and Taylor 1981), and very recently the relevance of such solutions to outbursts in binary systems has been recognized (MM1, MM2, MM4; Smak 1982a, b, 1983a, b; CGW; FLP, PFL; Mineshige and Osaki 1983).

MM2 present steady-state solutions obtained by integrating the disk equations and incorporating realistic opacities and a mixing-length theory of convection. They use a slightly modified α -theory [$\alpha \rightarrow \alpha(1 - 2d \ln P/d \ln z)$] which is negligibly

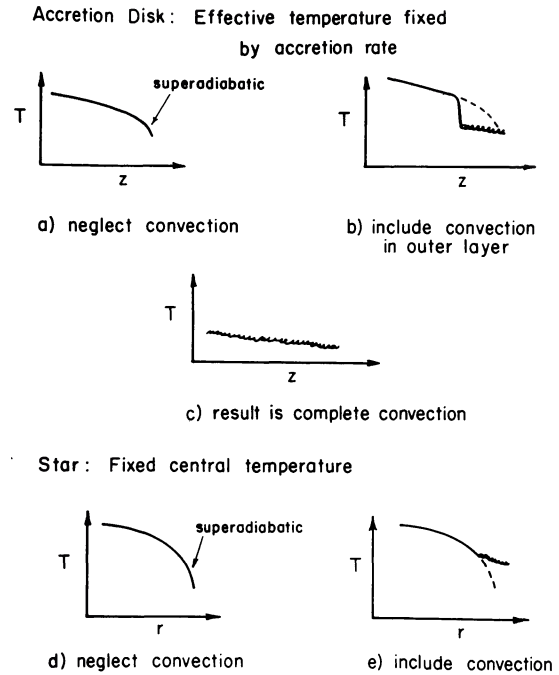


FIG. 1.—Schematic representation of the difference convection has on accretion disks (with fixed surface temperature) and stars (with fixed central temperature). In accretion disks, a small amount of convection near the surface in a pure radiative treatment may force the midplane temperature to a much lower value after convection is correctly included. By contrast, if one were constructing a stellar model with fixed central temperature, convection near the surface decreases the outer temperature while leaving the interior temperature unaffected.

different from simple α -theory. Their opacities are from Cox and Stewart (1969) and so do not include the effects of molecules. Their parameter study consists of steady-state solutions for $6.5 \leq \log r(\text{cm}) \leq 11$ and $\dot{M}(M_{\odot} \text{ yr}^{-1}) = 10^{-11}, 10^{-9}$, and 10^{-7} . They considered $\alpha = 1/(10\sqrt{2})$ for all three rates of accretion, with the $\dot{M} = 10^{-9} M_{\odot} \text{ yr}^{-1}$ track repeated for $\alpha = 3/(100\sqrt{2})$. Our results for this region of parameter space agree well with theirs (see the more detailed discussion in § III).

Smak (1982a) and Vila (1978) also perform explicit vertical integrations of the disk equations but take $\alpha = 0$ where convective energy transport is absent. They thus assume that only convection can induce viscosity. Smak showed that this assumption always leads to midplane convection. Vila's conclusion that convective viscosity alone cannot provide the accretion rates relevant for cataclysmic variables seems to ignore this midplane convection.

c) Instabilities

Piran (1978) has derived necessary conditions for the stability of vertically averaged accretion disk structure. These conditions depend on the logarithmic derivatives of cooling and viscosity with respect to disk thickness and surface density. They are generalized expressions of a linear instability analysis done by Shakura and Sunyaev (1976) for α -viscosity heating. In general, disks may suffer two kinds of instability. The

Lightman-Eardley (Lightman and Eardley 1974) instability causes the surface density to clump into alternately high and low density rings on a viscous time scale; a thermal instability causes the disk to contract or expand vertically on a thermal time scale while maintaining constant surface density. The viscous instability occurs when the vertically integrated stress is inversely related to surface density, and the thermal instability when heating and cooling are out of balance. An unstable structure will commonly be subject to both sorts of instabilities. The vertical thermal adjustment time scale is of order $1/\alpha\Omega$, and the viscous evolution time scale is larger by a factor of $(r/h)^2$, so that whenever an annulus goes from one temperature to another because of a thermal instability, this transition is rapid compared to the subsequent viscous response of the disk in the \hat{r} direction. The time scale for the entire disk to go from one viscosity state to another is uncertain at present.

The stability of steady-state models is indicated by the dependence of the surface density on some measure of the integrated stress, such as the mass accretion rate, flux, or central or surface temperature. For optically thick conditions, a sequence of steady-state models at constant radius for which the surface density decreases with increasing effective temperature is thermally unstable because a perturbation to larger temperature or density will induce conditions for which the heating dominates the cooling. If the unstable sequence connects to stable sequences (surface density increasing with effective temperature) at higher and lower temperatures, the resulting double-valued nature of the locus ensures that other stable solutions at higher or lower temperature are accessible at fixed surface density. The unstable portion is inaccessible to evolving disks as explained by Bath and Pringle (1982) and others. In general, the existence of an unstable sequence can give rise to limit cycle behavior (Pringle 1981).

In a plot of effective temperature versus surface density the locus of vertically explicit steady-state α -models at a single radius shows a characteristic "S-shaped" curve containing an unstable portion with negative slope (see Figs. 4 and 11; MM1, MM2; Smak 1982*a*, CGW; FLP). The factors affecting the shape of these curves will be discussed in detail in the next section. The instability occurs at an effective temperature of 5000–6000 K. It is related to the partial ionization of hydrogen which results in very temperature sensitive diffusive or convective flux. MM1 proposed a limit cycle mechanism for dwarf novae based on this unstable sequence and presented power-law scalings for burst energies, durations, and recurrence times in terms of α and the mass transfer rate from the companion, \dot{M}_T . With his models which neglect viscosity in radiative regions, Smak (1982*a*) also discovered such an S-shaped behavior induced by partial ionization in steady-state curves and independently discussed its relevance to dwarf nova outbursts.

CGW claimed this mechanism could only produce frequent, low-energy bursts. They argued that viscosity could plausibly be expected to increase with the outbreak of convection in cold models, ~ 2000 K, and that this would also induce instability. They proposed an ad hoc change in α in convective regions in order to get an appropriate S-shaped structure which could account quantitatively as well as qualitatively for

the observations of dwarf novae. For given r and \dot{M} one gets a larger surface density by making α smaller, so decreasing α substantially in the lower temperature radiative solutions produces a surface density enhancement that dominates the one discussed by MM1, MM2, and Smak (1982*a*).

The vertical integrations of Kozłowski, Wiita, and Paczyński (1979) are not based on α -theory. They have included realistic opacities, equation of state, and treatment of convection, but the assumption is made that the ratio of self-gravity to the gravity of the central object, $A = 2\pi G\Sigma/\Omega^2 h$, is a constant. This replaces an explicit prescription for viscosity. The resulting steady-state solutions are completely stable. When plotted in the $\log T_{\text{eff}} - \log \Sigma$ plane, they do not show the S-shape characteristic of α -theory solutions near $T_{\text{eff}} = 6000$ K. This is because at constant r and A , Σ must be proportional to the scale height, h , but h is proportional to $T_{\text{mid}}^{1/2}$ (where T_{mid} is the temperature at the disk midplane), independent of the viscosity. Thus, the surface density must increase monotonically with the midplane and effective temperatures in such models, and they will always be formally stable. There is no direct physical argument to show that this implicit treatment of viscosity is wrong. On the contrary, these models show how sensitive the results can be to differing treatments of the viscosity. The fact that this class of models cannot account for the dwarf nova instability may be an argument against them, again setting some constraints on the physical nature of the viscosity.

One has the following general picture of the instability limit cycle in dwarf novae suggested by the α -models which has recently been explored in detail by PFL, Smak (1983*a*), Mineshige and Osaki (1983), and MM4. Material in quiescence piles up in a broad ring at $\sim 3 \times 10^{10}$ cm from the white dwarf (Hensler 1982*a, b*). When the surface density anywhere in the ring exceeds some critical value, $\Sigma_{\text{max}}(r, \alpha)$, that portion of the ring goes to the hot state on the local thermal time scale, and thickens vertically. Heat will then be diffused to adjoining annuli initially on a radial thermal time scale. This time scale is given approximately by

$$\begin{aligned} \tau_r &= 9/32 \Sigma^2 (\delta r/h)^2 \kappa R / acT^3 \mu \\ &= \sim 3 \text{ hr} (\Sigma/100 \text{ g cm}^{-2})^2 (\delta r/h)^2 \\ &\quad \times (\kappa/10 \text{ cm}^2 \text{ g}^{-1}) / (T/10^4 \text{ K})^{-3}, \end{aligned} \quad (8)$$

where κ and T are representative midplane averages between the cold and hot state. Adjoining matter is heated by a combination of thermal and viscous effects and also ends up in the higher viscosity state. This higher viscosity material will rapidly form a disk which clears out in the course of the eruption.

The disk formed during outburst has a structure approximating that in steady state for which $\Sigma \propto r^{-3/4}$. The critical density for cooling, Σ_{min} , is proportional to radius (see § III*biv*). This means the outer disk edge will first attain $\Sigma < \Sigma_{\text{min}}$, and return to the low viscosity state. This transition will again be communicated to the rest of the disk, by radial diffusion and by perturbations in the surface density propa-

gated on a viscous time scale. In the low-viscosity quiescent stage, mass is once more stored up to power the next burst.

III. SURVEY OF PARAMETERIZED STEADY-STATE MODELS

a) Physical Assumptions

To construct vertically explicit disk structure we integrate the disk equations (1)–(3) using a Henyey (relaxation) algorithm. Both gas pressure and radiation pressure are included, as are components of vertical gravity from both the central object and disk. The ratio of self-gravity to central gravity is always small ($\sim 10^{-7}$). For our preliminary results (CGW) we treated convection merely by setting $\nabla = \min(\nabla, \nabla_{\text{ad}})$. For the present study we used the mixing-length theory (MLT) of convection (Schwarzschild 1958) taking $l = \min[z, (d \ln P/dz)^{-1} = H_p]$, where $z =$ height above mid-plane. These results are compared in § IIIbiii below with those of MM2 who use the Böhm-Vitense (1958) MLT of convection as described in Kippenhahn *et al.* (1967).

For low accretion rates the solutions are optically thin. We treat these states by considering the disk to be a plane-parallel slab locally with continuum optical depth given by $\tau = \int \kappa \rho dz$, where κ is the Rosseland mean opacity. Then, replacing the appropriate frequency-dependent equation with a frequency-independent one, the source function (taken to be the Planck function) is multiplied by $(1 - e^{-2\tau_{\text{mid}}})$ where $\tau_{\text{mid}} = \int_0^h d\tau$. This causes an elevation of the disk temperature, for the same r , \dot{M} , and α , over that were the low τ ignored (Tylenda 1981). Hence, optically thin solutions have higher temperatures than would optically thick solutions at the same rates of accretion. The Planck mean opacity $\kappa_P = (\pi/\sigma T^4) \int_0^\infty \kappa_\nu B_\nu(T) d\nu$ would be preferable for this approximation to the Rosseland mean opacity $\kappa_R^{-1} = (\pi/4\sigma T^3) \int_0^\infty \kappa_\nu^{-1} (\partial B_\nu/\partial T) d\nu$. Only the latter was readily available, however. This treatment also ignores potentially important radiative transfer effects in the optically thick lines, but as shown below our results for the locus of solutions with $\tau \approx 1$ agrees well with frequency-dependent calculations.

For $T > 10^4$ K we used opacities from the subroutine OPACIT supplied by B. Paczyński. It uses the opacities of Cox and Stewart (1969) supplemented by H_2O opacities from Auman (1966) and was originally intended to be valid for $T > 1500$ K. Recently, Alexander, Johnson, and Rypma (1983 AJR) have recalculated Rosseland mean opacities for $2.8 < \log T(\text{K}) < 4.0$ and included C_2 , CN, CO, H_2O , TiO, and other molecular species. Their opacities show a peak at $T \approx 2300$ K mainly due to H_2O and TiO. Figure 2 compares the AJR and Cox-Stewart opacities. Note that the H_2O peak is about a factor 5 larger than the corresponding OPACIT value. The bump in the AJR curves at $T \approx 4000$ K is from CN. The parameter study was originally done with the Cox-Stewart opacities and then the low-temperature portions repeated with the AJR opacities. For computations which pertain to the low-temperature convective/nonconvective critical points and the optically thin solutions the AJR opacity table was used.

The equation of state routine was supplied by H. Saio and uses the physics described by Iben (1963). It is used to determine the mean molecular weight μ and adiabatic temper-

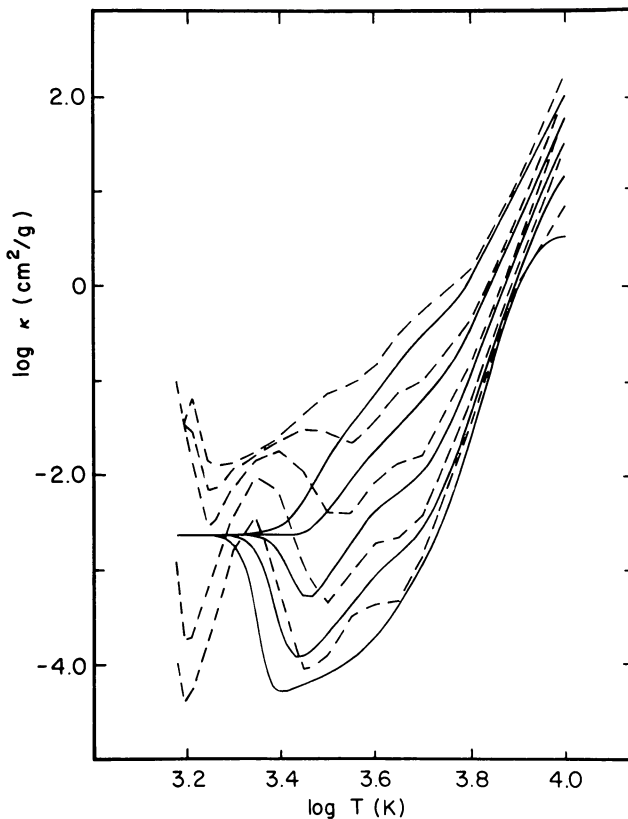


FIG. 2.—Rosseland mean opacities from Cox and Stewart (1969) and Auman (1966) (solid curve) and Alexander, Johnson, and Rypma (1983) (dashed curve) for $\log \rho(\text{g cm}^{-3}) = -6, -7, -8, -9, \text{ and } -10$, and $3.18 < \log T(\text{K}) < 4.00$ are compared. Alexander *et al.* opacities are larger at lower temperatures because of molecular absorbers. The only molecular contributor to the first set of opacities is H_2O . Alexander *et al.* opacities are about a factor of 5 larger than the former opacities at $\log T(\text{K}) \approx 3.3$.

ature gradient ∇_{ad} . The equation of state for determining partial abundances used by AJR has been used implicitly in their tabular opacities and so is independent and not necessarily consistent with the Saio routine. Fortunately, μ and ∇_{ad} depend almost entirely on whether hydrogen is mostly H_2 , H, or H^+ , whereas the opacity depends mainly on species with small fractional abundance such as H_2O , TiO, and CN. The physical state of the dominant hydrogen reservoir depends on these species only to second order. Figure 3 presents a plot of μ and ∇_{ad} versus $\log T$ for $\rho = 10^{-8} \text{ g cm}^{-3}$. Note ∇_{ad} decreases substantially at $\log T(\text{K}) = 3.4$ and 4.0 where H is partially dissociated and partially ionized, respectively. Note also that for $\log T(\text{K}) < 3.55$, ∇_{ad} is smaller than 0.4. The molecular hydrogen predominant at this temperature has two degrees of freedom in addition to the three translational degrees of a monatomic gas, so $\gamma = 7/5$ and $\nabla_{\text{ad}} = (\gamma - 1)/\gamma = 2/7$ (vs. $2/5$ for a monatomic gas).

For optically thick solutions we integrated beyond the photosphere to the actual disk surface ($\rho \approx 0$). If $\delta\tau$ is defined as the optical depth from disk surface inward, then the photosphere occurs at the vertical structure grid point where $\delta\tau = 2/3$. The temperature at this point is related to the surface flux given in equation (7) by $T_{\text{eff}} = (F_s/\sigma)^{1/4}$. Replacing the

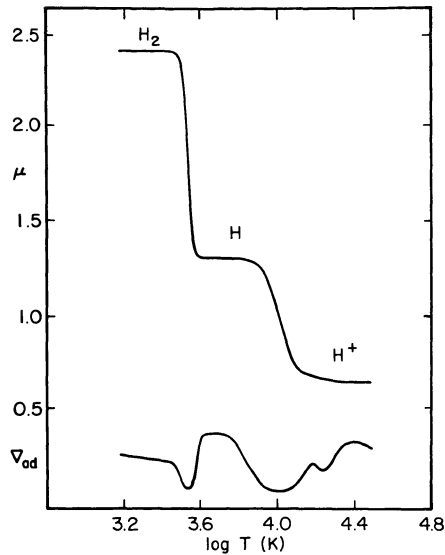


FIG. 3.—Mean molecular weight μ and adiabatic index $\nabla_{\text{ad}} = (d \ln T / d \ln P)_{\text{ad}}$ for $\rho = 10^{-8} \text{ g cm}^{-3}$. The increased number of degrees of freedom in a partly dissociated or partly ionized gas causes ∇_{ad} to decrease near $\log T(\text{K}) = 3.5$ and 4.0 . The small dip at $\log T(\text{K}) = 4.3$ is from partly ionized helium. This is from an equation of state routine kindly supplied by Hideyuki Saio.

diffusion equation

$$F = -4/3 ac / \kappa \rho T^3 dT / dz, \quad (9)$$

with a flux-limited diffusion equation

$$F = -ac / 3T^4 x / [1 + x(1/3 + e^{-x/2})] \quad (10)$$

(Alme and Wilson 1973; Chevalier 1981), where $x = 1 / \kappa \rho d / dz (\ln T^4)$, in the outermost grid points where $\delta \tau < 2/3$ has negligible effect on the results.

b) Results

Four main regimes are apparent in the steady-state solutions: (1) At very low rates of accretion the solutions are optically thin. (2) At higher rates of accretion the solutions become optically thick. (3) When the midplane temperature exceeds ~ 2200 K, midplane convection appears. As the accretion rate increases further, midplane convection increases and engulfs most of the vertical structure. A local maximum in Σ occurs at $T_{\text{eff}} \approx 4000\text{--}7000$ K. (4) At very high \dot{M} , solutions free of midplane convection appear. The latter two regimes have previously been studied in some detail by MM2.

We discuss these four regimes separately below and present power-law scalings for the surface density and temperature associated with these regions and for related critical points.

i) Optically Thin Solutions

Figure 4 shows three tracks for constant r and α which extend from very low to very high \dot{M} . The left-hand, approximately horizontal portions are optically thin. They were computed with a vertically averaged code using the structure equations (15) and (16) and AJR opacities. The right-hand,

vertical portions are optically thick. They were computed with the full vertical treatment detailed above. The connecting dashed points were not computed. The hash marks indicate the logarithms of accretion rate (in solar masses per year) and optical depth. The curve for $\alpha = 1.0$ turns optically thin at $T \approx 4500$ K, whereas the curve for $\alpha = 0.01$ stays optically thick down to far lower temperatures, ~ 1500 K. This is because midplane density and temperature scale inversely with α . For the same \dot{M} , solutions with lower α have higher optical depths.

The negative slopes of the optically thin curves can be understood quantitatively in terms of the vertically averaged method. Using the fact that optically thin solutions are isothermal, and combining the equations of state, flux, viscosity, and hydrostatic equilibrium, letting the source function $(1 - e^{-2\tau_{\text{mid}}})\sigma T^4$ go to $2\tau_{\text{mid}}\sigma T^4$ (since $\tau \ll 1$) and adopting

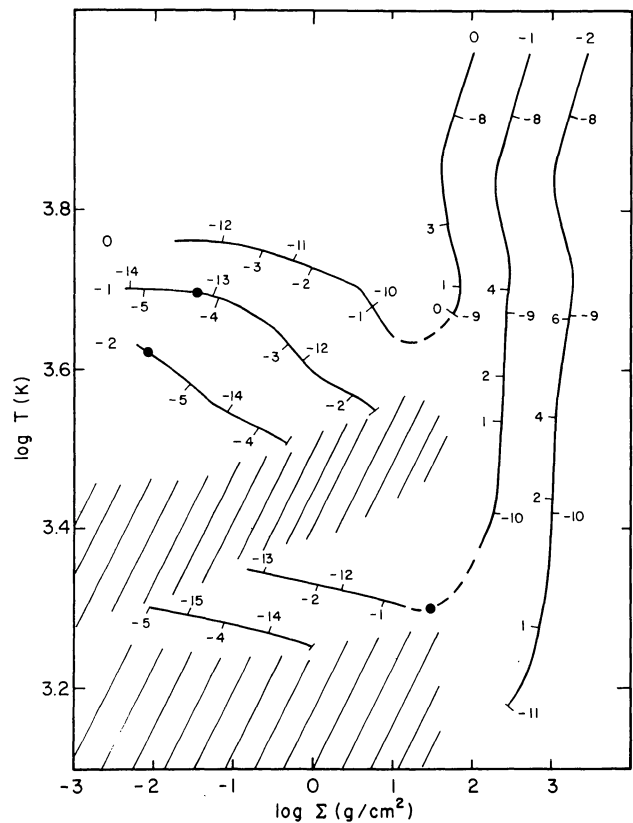


FIG. 4.—Three curves representing a series of steady-state solutions at $r = 10^{10.5} \text{ cm}$. In order of increasing surface density the curves are for $\alpha = 1.0, 0.1,$ and 0.01 . The log of α for each curve is indicated where the curve terminates at both low and high \dot{M} . Numbers to the right and above the curves are the log of mass accretion rate in solar masses per year. Numbers to the left and below the curves are the log of midplane to surface Rosseland mean optical depth. Isothermal disk temperature is shown for the optically thin curves, and effective temperature is shown for the optically thick curves. The optically thin curves are computed using a vertically averaged code described in § IIIb. Optically thick curves are computed using the full vertical treatment. Hatched regions indicate "forbidden" zones that are discussed in the text. Near the forbidden zone at $\log T(\text{K}) \approx 3.4$ the solutions are double-valued: for the same r, \dot{M} , and α two solutions exist. These solutions are to the right of the large dots on the upper branch and to the left of the large dot on the lower branch. The $\alpha = 0.01$ curve enters the lower forbidden region before this point.

an opacity law of the form

$$\kappa = \kappa_0 \rho^a T^b \quad (11)$$

gives

$$d \log T / d \log \dot{M} = a / (1.5a - b - 3), \quad (12)$$

$$d \log \Sigma / d \log \dot{M} = (a - 2b - 6) / (3a - 2b - 6), \quad (13)$$

and hence

$$d \log T / d \log \Sigma = 2a / (a - 2b - 6). \quad (14)$$

The Piran criterion for thermal stability is $(d \log C / d \log h)_\Sigma > (d \log H / d \log h)_\Sigma$, where C and H are heating and cooling functions, respectively. This criterion becomes $a - 2b - 6 < 0$, and the criterion for LE stability reduces to $3a - 2b - 6 < 0$. Note that these two inequalities, when inserted into equations (12)–(14) give $d \log T / d \log \dot{M} < 0$, $d \log \Sigma / d \log \dot{M} > 0$, and $d \log T / d \log \Sigma < 0$. These relations are obeyed by the optically thin solutions depicted in Figure 4. Opacity increases with density such that $a \approx 0.5$ – 1.0 ; hence, for general stability $b \geq -2$ to -3 . When opacity decreases sharply with temperature such that $b < -3$, “forbidden zones” appear. These will be discussed below. We were unable to obtain numerical solutions in these zones, but the existence of such solutions is moot since they are not only unstable but also unattainable.

Rewriting equations (12) and (13) leaving the opacity dependence explicit gives

$$\kappa T^3 = 3/4 \alpha R \Omega / \mu \sigma, \quad (15)$$

and

$$\rho T^{3/2} = \dot{M} \Omega^2 f / 4 \pi \alpha (\mu / R)^{3/2}, \quad (16)$$

where $f = [1 - \beta \sqrt{(r_{wd}/r)}]$. From this we see that for constant r and α , κT^3 is constant and $\rho T^{3/2} \propto \dot{M}$.

From equation (15), the locus of optically thin solutions for given r and α with varying \dot{M} can be characterized by a straight line of slope -3 in the opacity plane (Fig. 3). For $\alpha \approx 1$ the optically thin solutions only exist for $\log T(\text{K}) \geq 3.6$ because decreasing T leads to larger κ and optically thick conditions where equations (15) and (16) are invalid. The optically thin solution for $\alpha = 1.0$ depicted in Figure 4 is consistent with this criterion. For smaller α the solutions can be double-valued, with a high-temperature branch of optically thin solutions separated from a low-temperature branch [$\log T(\text{K}) \leq 3.4$] by a “forbidden” region where optically thin solutions do not exist as a result of the decrease of opacity with temperature, as just discussed. These two optically thin branches and the “forbidden” region are also illustrated in Figure 4 by the curves for $\alpha = 1.0, 0.1$, and 0.01 . The nature of the cold branch depends critically on the effect of molecules which produce the peak in opacity at $\log T(\text{K}) \approx 3.3$. Note that the existence of the “forbidden” optically thin zone means, for example, that for $\alpha \leq 0.1$ and $\Sigma \geq 10 \text{ g cm}^{-2}$ the only steady-state solutions are at $\log T(\text{K}) \leq 3.4$. For given α ,

the optically thin branches are shifted to higher temperatures as one goes to smaller r .

If the quantity κT^3 is greater than some amount, the forbidden region disappears because $d \log \kappa / d \log T > -3$ everywhere on the optically thin locus of solutions, and hence all steady-state solutions are stable. From Figure 2 this occurs at roughly $(\kappa \text{ cm}^2 \text{ g}^{-1})(T/10^{3.1} \text{ K})^3 \approx 0.63$. Hence, one has from equation (15) that for $3/4 \alpha R \Omega / \mu \sigma \geq (\kappa T^3)_{\text{crit}} \approx 10^{9.1}$ or $\alpha \geq 0.1 \mu r_{10}^{3/2}$ there is only one branch of optically thin solutions. If α is less than this critical value, there is no warm optically thin state in thermal equilibrium, and the gas must cool to $\log T(\text{K}) < 3.4$. For $r = 3 \times 10^{10} \text{ cm}$ a warm, optically thin, single-valued solution is only accessible if $\alpha \geq 0.7$. For $r = 10^{10} \text{ cm}$ the critical value of α is 0.13 . The critical value of α is less than 0.1 only for $r \leq 7 \times 10^9 \text{ cm}$.

The nature of these optically thin solutions implies that for α only moderately less than unity, the only steady-state solution with $\Sigma < \Sigma_{\text{min}}$ is cool: $T \leq 10^{3.4} \text{ K}$ at the outer edge of a standard dwarf nova disk where $r_{10} \approx 3$. Such a low-temperature solution will have a long viscous time scale and a low accretion rate. At smaller radii warm, optically thin portions can remain in thermal equilibrium, but they will not build back up toward a critical density because they have a relatively high accretion rate and the flow from the companion star will be choked off by the outer, cooler, low viscosity regions. The warm, inner portions will be drained of matter during quiescence until they reach the low accretion rate corresponding to the outer, cool material, or until another outburst begins. If the cooler portions have lower α , this tendency to form a distinct cool ring which chokes the flow to inner portions of the disk will be exacerbated. Such a ring will be the natural site of the next outburst.

On either side of the forbidden zone at $\log T(\text{K}) \sim 3.4$ there is a range of Σ where, for the same r , \dot{M} , and α , two solutions are possible. The portions of the optically thin branches for which this is true lie between the large dots on the hot and cold curves in Figure 4.

At very low temperatures [$\log T(\text{K}) \leq 3.25$] another forbidden region appears as dust absorption causes the opacity to increase. This occurs for large r and small α , and prevents the optically thin branch at $3.25 < \log T(\text{K}) < 3.3$ for $\alpha = 0.01$ shown in Figure 4 from connecting directly to the optically thick curve. Were an evolving ring of material to encounter these conditions, it would cool until it entered a region where $d \log \kappa / d \log T > -3$ and then be in steady state. From the AJR opacities the next such state occurs at $T \leq 1000 \text{ K}$.

Tylenda (1981) presents vertically averaged steady-state α -disk solutions computed with frequency-dependent opacities. For $\alpha = 1.0$ and several rates of accretion he calculates the radius for which his solutions become optically thin (see Tylenda 1981; p. 133; Fig. 1.) This is indicated by an increase of the disk temperature over that expected from the optically thick expression $\sigma T_{\text{eff}}^4 = F_s$. The locus of points of departure from optically thick conditions is given roughly by

$$T(\text{K}) = 5800 - 1800[\log r(\text{cm}) - 10]. \quad (17)$$

Assuming these points correspond approximately to $\tau_{\text{mid}} = 2$, we computed solutions for $10 < \log r(\text{cm}) < 11$, $\alpha = 1$, and τ_{mid}

in this range. For Cox-Stewart opacities the effective temperatures corresponding to $\tau_{\text{mid}} = 2$ are $\sim 2\%$ – 3% higher than that given by equation (17), whereas with the larger AJR opacities the effective temperatures are 5% – 10% lower than equation (17). This close agreement with a frequency-dependent study adds strength to our optically thin treatment.

ii) Cool Radiative Solutions

The vertical structure of cold radiative solutions just before the onset of convection is illustrated in Figures 5a and 5b for $r = 3 \times 10^{10}$ cm and for $\alpha = 1.0$ and 0.01 , respectively. The structures correspond to the points at 10^{-9} and 10^{-11} $M_{\odot} \text{ yr}^{-1}$ in two of the curves of Figure 4. The optical depth is slightly greater than unity. Note that the solutions are nearly isothermal, but the slight temperature gradient signals the approach to convective instability. The decline of density and pressure is only slightly steeper than the Gaussian form characteristic of a perfectly isothermal structure.

Even though the location in parameter space of the first appearance of midplane convection is a complicated function of the vertical structure, one can write down the necessary condition for midplane convection to occur as a mixed expression containing r , α , ρ_{mid} , and T_{mid} . Combining the equations of radiative transport and hydrostatic equilibrium and using l'Hopital's rule gives

$$\nabla = d \log T / d \log P = 9/32 \alpha / \sigma \Omega \kappa (\rho R / \mu T)^2, \quad (18)$$

where all variables are evaluated at the midplane. When this quantity exceeds ∇_{ad} , the Schwarzschild inequality for convection is satisfied.

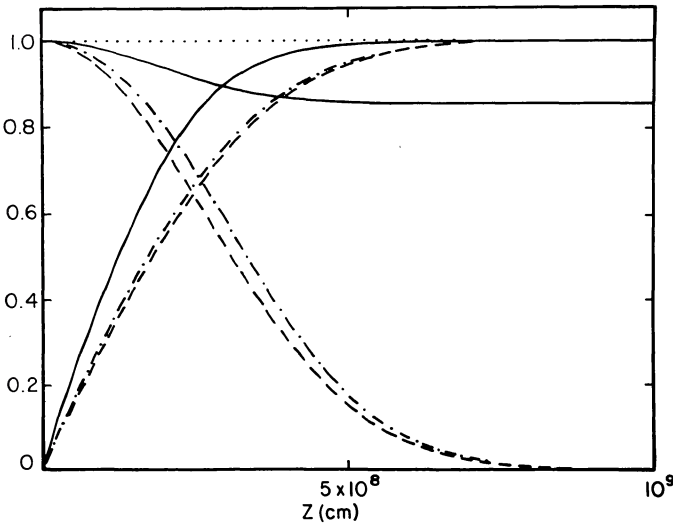


FIG. 5a

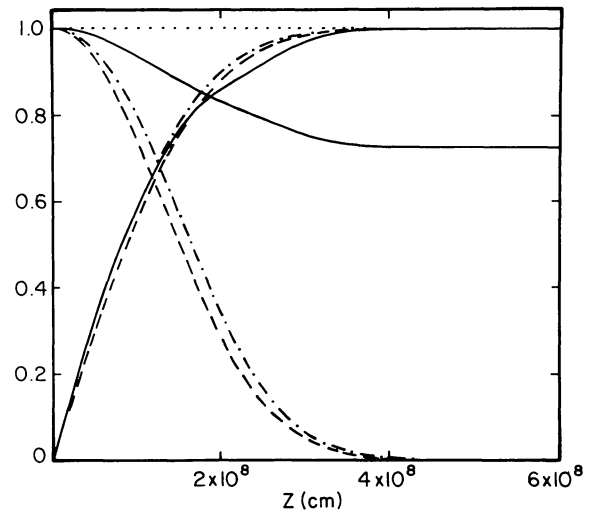


FIG. 5b

FIG. 5.—(a) Vertical structure of a cold radiative solution. Quantities are shown in terms of either their midplane or surface values. Of the three ascending curves, the solid one is optical depth, the dashed one is surface density, and the dash-dotted is flux. Of the three descending curves, the solid one is temperature, the dashed one is pressure, and the dash-dotted one is density. Dotted curve is $F_{\text{radiative}}/F_{\text{total}}$; $\alpha = 1.0$, $r = 10^{10.5}$ cm, and $\dot{M} = 10^{-9.00} M_{\odot} \text{ yr}^{-1}$. Maximum values of the quantities shown are $\tau_{\text{mid}} = 1.85$, $\Sigma = 61.3 \text{ g cm}^{-2}$, $F_s = 2.76 \times 10^{10} \text{ ergs cm}^{-2} \text{ s}^{-1}$, $T_{\text{mid}} = 4947 \text{ K}$ ($T_s = 4219 \text{ K}$), $P_{\text{mid}} = 2.77 \times 10^4 \text{ dyn cm}^{-2}$, and $\rho_{\text{mid}} = 8.76 \times 10^{-8} \text{ g cm}^{-3}$. The structure is nearly isothermal because of its low optical depth. (b) Vertical structure of a cold radiative solution; $\alpha = 0.01$, $r = 10^{10.5}$ cm, and $\dot{M} = 10^{-10.69} M_{\odot} \text{ yr}^{-1}$. Curve designations are the same as in (a). Maximum values of the quantities shown are $\tau_{\text{mid}} = 4.04$, $\Sigma = 533 \text{ g cm}^{-2}$, $F_s = 5.64 \times 10^8 \text{ ergs cm}^{-2} \text{ s}^{-1}$, $T_{\text{mid}} = 2160 \text{ K}$ ($T_s = 1564 \text{ K}$), $P_{\text{mid}} = 1.17 \times 10^5 \text{ dyn cm}^{-2}$, and $\rho_{\text{mid}} = 1.56 \times 10^{-6} \text{ g cm}^{-3}$. As for the cold $\alpha = 1$ solution, T_{mid} and T_s approach each other as the optical depth decreases.

From the numerical steady-state solutions approximate power-law scalings can be obtained for the point where, for a series of solutions of increasing \dot{M} and constant r and α , midplane convection first appears. Concurrent with this onset of convection is an increase in optical depth and midplane partial ionization. A numerical subscript x here and below on r , \dot{M} , or T indicates that that parameter is expressed in units of 10^x times cm, $M_{\odot} \text{ yr}^{-1}$, or K, respectively. For Cox-Stewart opacities the scalings are as follows. For $r \approx 10^{10}$ cm and $\alpha \approx 10^{-2}$ we find

$$T_{\text{mid,conv}} \sim 3300 \text{ K } r_{10}^{-0.1} \alpha_{-2}^{0.1}, \quad (19)$$

and

$$\Sigma_{\text{conv}} \approx 400 \text{ g cm}^{-2} r_{10}^{1.15} \alpha_{-2}^{-0.66}. \quad (20)$$

For larger r these scalings break down. Beyond $r \approx 10^{11}$ cm the exponents of both r and α are about one-third smaller. With the AJR opacities there is a broad region of parameter space over which the following power-law scaling for this critical value of Σ is quite accurate:

$$\Sigma_{\text{conv}} = 220 \text{ g cm}^{-2} r_{10}^{0.76} \alpha_{-2}^{-0.49}. \quad (21)$$

This differs from equation (20) because of the different dependencies of κ on ρ and T between the AJR and the Cox-Stewart opacities. The uniform scaling is apparent over the range of r and α shown in Figure 6.

With the AJR opacities, the midplane temperature at the onset of convection cannot be written as a general power law.

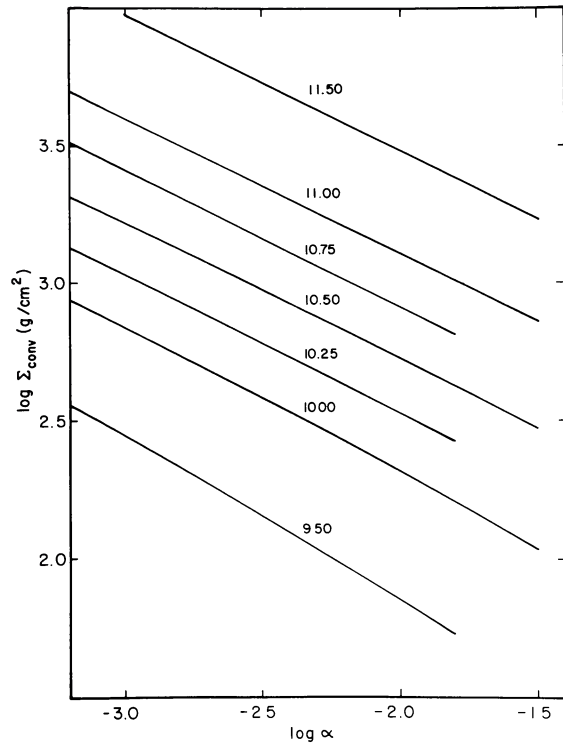


FIG. 6.—Surface density of solutions where midplane convection first appears as a function of α for varying radii. Numbers over each curve are $\log r(\text{cm})$. Curves are described to good accuracy by the power-law scaling given in text.

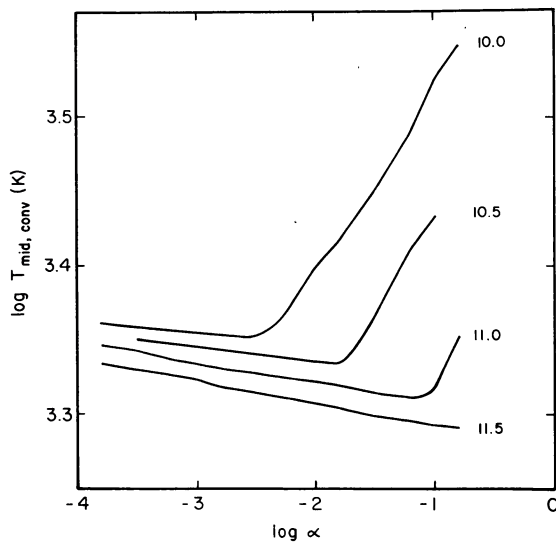


FIG. 7.—Midplane temperature of solutions where midplane convection first appears as a function of α for varying radii. Numbers to the right of each curve are $\log r(\text{cm})$. For large α and small r the opacity is steeply increasing with T as the midplane becomes partially ionized. For small α and large r the midplane temperatures are lower and material is neutral.

Figure 7 shows how the midplane temperature depends on α and r for this case. Note that it is not a monotonic function of α as it was for the Cox-Stewart opacities. The change in slope displayed in Figure 7 occurs where the opacity changes from having a weak to a strong dependence on temperature. Consider, for example, what happens to the convective critical point at one radius r as α is increased: e.g., starting at $\alpha = 10^{-4}$ and $r = 10^{10.5}$ cm. From equation (18) for ∇_{mid} the quantity $[\alpha\kappa(\rho/T)^2]_{\text{mid}}$ is constant for this sequence of solutions. One finds that as α increases, κ and T are nearly constant (they decrease by a small amount); hence, ρ must decrease approximately as the square root of α . Starting at about $\alpha = 10^{-1.8}$, however, the opacity begins to increase with temperature. The density decrease is now insufficient to balance the increase of $\alpha\kappa$, so T must increase. This change occurs at larger α for larger r since the density is less. Note in Figure 6 the relative change in the dependence of Σ_{conv} on α is small as this transition is made.

More details of the physical conditions at the onset of midplane convection are given in Table 1. The rate of accretion at these solutions is 0.01 dex below that at which a trace of superadiabaticity develops at the midplane. Note that for given r the rate of accretion for these points is higher for higher α . This occurs for the following reason. If r and \dot{M} are held constant and α increases, the midplane temperature T_{mid} of a steady-state solution increases. However, at $T \approx 2000$ – 2200 K and $\rho \approx 10^{-6}$ g cm $^{-3}$, Figure 2 shows that the opacity is starting to increase with temperature, so that solutions with this midplane temperature are beginning to have a large temperature gradient and hence midplane convection, independent of the value of α . Thus solutions at this critical point at which midplane convection is just starting represent approximately a locus of constant $T_{\text{mid}} \approx 2000$ K. To increase α at constant T_{mid} requires the rate of accretion to increase. That T_{mid} is not exactly constant reflects the weak density dependence of the opacity. In summary, the onset of midplane convection using the AJR opacities is caused by the increase in opacity at $T \approx 2000$ K and hence $T_{\text{mid,conv}} \approx 2000$ K with small regard for α . Keeping $T_{\text{mid,conv}}$ roughly constant in this fashion and raising α causes Σ_{conv} to decrease.

The AJR opacities give lower rates of accretion associated with these critical points for midplane convection than originally reported (CGW Fig. 2). This is a consequence of the new larger opacities. Lower \dot{M} is required for the midplane temperature gradient to be small enough to be convectively stable. Note that solutions with smaller α have larger optical depths. This is because ρ and α are inversely related. CGW also reported that $\tau \approx 1$ at the points where convection starts. Those results were based on $\alpha \approx 0.01$, however, and it is now apparent with a more complete coverage of parameter space that this is not true in general.

The low-temperature convective instability mechanism of CGW depends critically on having a small α in the low-temperature, radiative regimes. The idea of using steady-state α -solutions to describe a cold, low-viscosity state of course ignores radial energy transport and the radial pressure gradient as mentioned previously. Hence, these results are probably only approximately correct for the purpose of describing a radially extended, low-viscosity disk state. In particular, when

TABLE 1
CONDITIONS AT THE ONSET OF MIDPLANE CONVECTION

	$-\log \alpha$	$-\log \dot{M} (M_{\odot} \text{ yr}^{-1})$	Σ (g cm^{-2})	T_{mid} (K)	T_{eff} (K)	τ_{mid}	h/r ($\rho/\rho_{\text{mid}}=1\%$)
11.50	3.5	9.24	16750.	2140	747	149.	0.0364
	3.0	8.99	9531.	2111	862	79.2	0.0364
	2.5	8.75	5338.	2062	990	40.6	0.0360
	2.0	8.50	3041.	2028	1143	20.8	0.0357
	1.5	8.25	1734.	1990	1321	10.3	0.0357
11.25	3.0	9.55	6081.	2127	959	52.6	0.0273
	2.5	9.30	3467.	2097	1109	27.5	0.0273
	2.0	9.05	1974.	2065	1279	14.2	0.0273
11.00	3.5	10.34	7038.	2205	933	68.6	0.0207
	3.0	10.10	3943.	2156	1071	35.4	0.0206
	2.5	9.85	2244.	2128	1237	18.7	0.0206
	2.0	9.60	1276.	2097	1428	9.49	0.0207
	1.5	9.35	726.0	2065	1649	4.59	0.0212
10.75	3.0	10.64	2581.	2199	1201	24.2	0.0156
	2.5	10.40	1445.	2151	1379	12.3	0.0156
	2.0	10.15	821.0	2124	1592	6.19	0.0159
10.50	3.5	11.44	2893.	2246	1157	30.0	0.0118
	3.0	11.19	1648.	2218	1336	15.9	0.0118
	2.5	10.94	938.8	2187	1542	8.13	0.0119
	2.0	10.69	532.7	2161	1781	3.96	0.0122
	1.5	10.41	296.1	2323	2097	2.43	0.0126
10.25	3.0	11.73	1060.	2241	1489	10.4	8.94 - 3
	2.5	11.48	602.8	2214	1719	5.21	9.11 - 3
	2.0	11.22	338.8	2250	1999	2.65	9.22 - 3
10.00	3.5	12.51	1204.	2288	1438	13.2	6.74 - 3
	3.0	12.26	683.1	2267	1660	6.74	6.83 - 3
	2.5	12.01	385.8	2249	1958	3.26	6.82 - 3
	2.0	11.72	211.9	2505	2271	2.36	7.37 - 3
	1.5	11.46	107.3	2825	2646	1.93	7.93 - 3
9.75	3.0	12.78	437.3	2284	1849	4.21	5.26 - 3
	2.5	12.51	243.4	2400	2163	2.44	5.41 - 3
	2.0	12.25	123.6	2697	2520	1.95	5.81 - 3
9.50	4.0	13.77	890.1	2341	1550	10.6	3.86 - 3
	3.5	13.52	502.4	2328	1789	5.41	3.86 - 3
	3.0	13.27	279.2	2342	2069	2.70	3.98 - 3
	2.5	13.01	144.0	2592	2411	2.01	4.27 - 3
	2.0	12.77	70.03	2913	2780	1.69	4.55 - 3

α is smaller than $h/r \approx 10^{-2}$, the α -theory formalism of decoupling the vertical structure differential equations from the r -structure equations becomes questionable. This was recently pointed out by Kippenhahn and Thomas (1982). When $\alpha < h/r$, the time scale for hydrostatic equilibrium to maintain itself in the \hat{r} direction is shorter than the thermal time scale in the disk; i.e., hydrostatic equilibrium prevails in both the \hat{r} and \hat{z} directions. Pressure and density therefore must remain constant on lines of constant effective potential. For $z \ll r$ this potential is given by $\psi \approx 1/2GM z^2/r^3$. In particular, the midplane is a surface of constant potential. Hence, α -theory solutions, which give $d \log P/d \log r$ and $d \log \rho/d \log r < 0$, are inconsistent. Kippenhahn and Thomas conclude, however, that a small baroclinicity (variation of orbital speed v_{ϕ} with z) produced by weak meridional

flow alters the structure of this effective potential. Thus, α -theory may not suffer badly from this particular kind of a fundamental inconsistency.

iii) Solutions with Hydrogen Recombination

The S-shaped features near $T \approx 10^{3.8}$ K, as shown on the rising portion of the curves in Figure 4, are associated with the partial ionization of hydrogen at this temperature. There are two principal phenomena that combine to cause a nonmonotonic relation between effective temperature and surface density. One is the rapid variation of opacity as hydrogen recombines, and the other is the convection associated with the large opacity. We shall denote these $\Sigma_{\text{max},1}$ and $\Sigma_{\text{max},2}$, respectively. The increase in opacity at small optical depths due to H_2O and TiO can also have a minor effect.

Combining the steady-state equations of flux and viscosity gives

$$9/8 \nu_{\text{mid}} \Sigma \Omega^2 = 3/4 \alpha R / \mu T_{\text{mid}} \Sigma \Omega = \sigma T_{\text{eff}}^4. \quad (22)$$

Note that T_{mid} need only be proportional to the fourth power of T_{eff} to have Σ and T_{eff} inversely related to each other and hence give a negatively sloping curve. We will see how the phenomena mentioned above can lead to a steep dependence of T_{mid} on T_{eff} .

For $\alpha \geq 0.3$, the increase in surface density as the effective temperature decreases is caused by the rapid decrease in opacity as hydrogen recombines. This effect comes in at $T_{\text{mid}} < 10^4$ K and $T_{\text{eff}} < 4000$ – 7000 K, depending on r , and is caused by the following. Even with convection present, the midplane and effective temperatures are approximately related by the diffusion equation $T_{\text{mid}} \approx \tau_{\text{mid}}^{1/4} T_{\text{eff}}$ in this regime. Since the opacity decreases as $\sim T^{-10}$ for $T < 10^4$ K, the midplane temperature drops precipitously as the effective temperature decreases. From equation (22), the surface density is forced to increase to maintain thermal equilibrium. When the opacity begins to drop less steeply with temperature, around 4000 – 6000 K as shown in Figure 2, the midplane temperature is not as sensitive to the effective temperature, and the surface density begins to decrease with decreasing effective temperature once more, causing $\Sigma_{\text{max},1}$. Hence, although these solutions have convection present, it is not the cause of the Σ inversion.

For $\alpha < 0.3$ the increase in Σ as the effective temperature decreases is caused by strong convection which lowers the temperature gradient drastically. This causes the required steep dependence of T_{mid} on T_{eff} and induces $\Sigma_{\text{max},2}$. This effect comes in at about the same T_{eff} as before, but now $T_{\text{mid}} \approx 17,000$ K. The reason convection is more important for low- α solutions will be explained below. The Σ reversal associated with T_{mid} dropping below 10^4 K ($\Sigma_{\text{max},1}$) is still seen, but it now occurs at lower T_{eff} (see Fig. 11).

Figures 8a and 8b depict the vertical structure of models on the optically thick negatively sloping portions of the $\log T_{\text{eff}} - \log \Sigma$ curves of Figure 4 for $r = 3 \times 10^{10}$ cm and for $\alpha = 1.0$ and 0.01 , respectively. Note that there is a density inversion due to convection just as one finds in layers of partial ionization in stars (Chitre and Shaviv 1967; Joss, Salpeter, and Ostriker 1973). The pressure gradient depends only on ρg_z , which changes slowly (even where convection is occurring). The temperature gradient is quite steep, however, because of the large superadiabaticity. Hence, given that $P \propto \rho T$, ρ increases if T decreases too fast. Figures 8a and 8b show that convective energy transport is sluggish at the midplane where material is in free fall (in an orbiting reference frame). This is in contrast with stars where the higher core densities promote efficient convection. A short distance above the midplane convection is carrying all but one part in 10^2 – 10^4 of the total flux. Convection carries a smaller portion of the total flux at its maximum efficiency for the solution with $\alpha = 1.0$, so the temperature gradient is larger, and the density inversion is

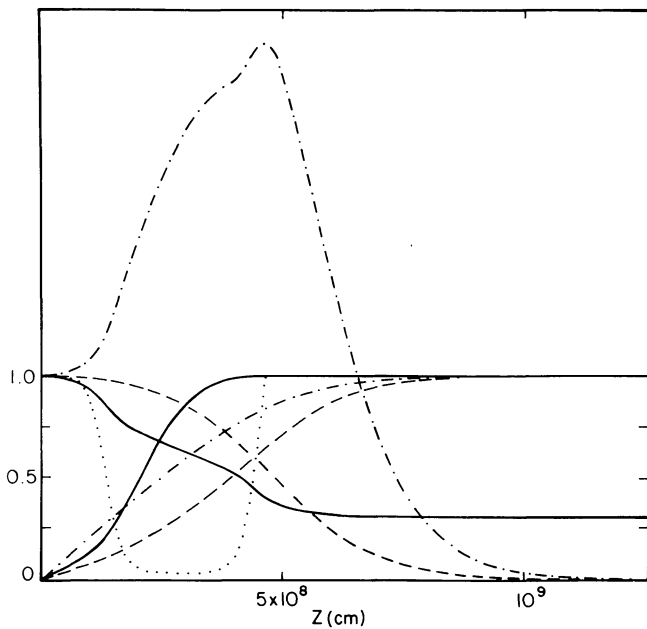


FIG. 8a

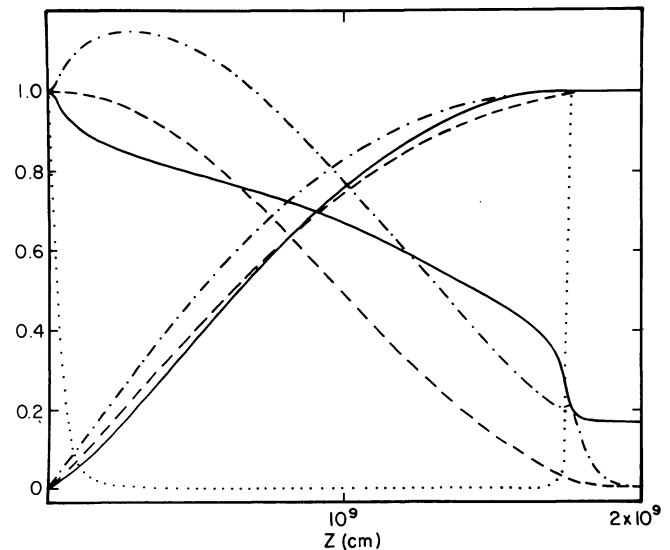


FIG. 8b

FIG. 8.—(a) Vertical structure of a solution between Σ_{min} and Σ_{max} ; $\alpha = 1.0$, $r = 10^{10.5}$ cm, and $\dot{M} = 10^{-8.60} M_{\odot} \text{ yr}^{-1}$. Curve designations are the same as in Fig. 5a. Maximum values of the quantities shown are $\tau_{\text{mid}} = 1740$, $\Sigma = 56.9 \text{ g cm}^{-2}$, $F_s = 6.93 \times 10^{10} \text{ ergs cm}^{-2} \text{ s}^{-1}$, $T_{\text{mid}} = 17,350 \text{ K}$ ($T_s = 5191 \text{ K}$), $P_{\text{mid}} = 4.80 \times 10^4 \text{ dyn cm}^{-2}$, and $\rho_{\text{mid}} = 2.20 \times 10^{-8} \text{ g cm}^{-3}$. The “opacity peak” convection is more extensive than in Fig. 13a. Convective energy transport weakens as one nears the midplane since $v_{\text{conv}} \propto (g_z)^{1/2} z = O(z^{3/2})$. One sees a density inversion because of the steep temperature gradient. Minimum value of $F_{\text{rad}}/F_{\text{tot}}$ is 0.028. (b) Vertical structure of a solution between Σ_{min} and Σ_{max} ; $\alpha = 0.01$, $r = 10^{10.5}$ cm, and $\dot{M} = 10^{-8.60} M_{\odot} \text{ yr}^{-1}$. Curve designations are the same as in (a). Maximum values of the quantities shown are $\tau_{\text{mid}} = 6.43 \times 10^5$, $\Sigma = 1580 \text{ g cm}^{-2}$, $F_s = 6.93 \times 10^{10} \text{ ergs cm}^{-2} \text{ s}^{-1}$, $T_{\text{mid}} = 32,060 \text{ K}$ ($T_s = 5191 \text{ K}$), $P_{\text{mid}} = 2.30 \times 10^6 \text{ dyn cm}^{-2}$, and $\rho_{\text{mid}} = 5.64 \times 10^{-7} \text{ g cm}^{-3}$. The structure has strong convection which extends almost to the photosphere ($T_{\text{eff}} = 5930 \text{ K}$). Minimum value of $F_{\text{rad}}/F_{\text{tot}}$ is 1.15×10^{-3} .

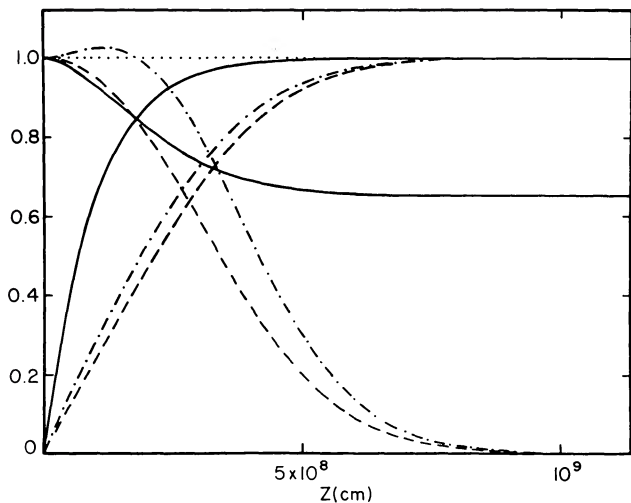


FIG. 9a

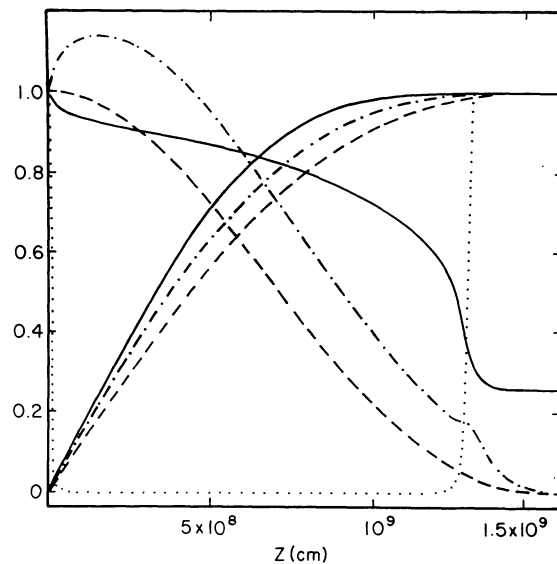


FIG. 9b

FIG. 9.—(a) Vertical structure of a Σ_{\max} solution; $\alpha = 1.0$, $r = 10^{10.5}$ cm, and $\dot{M} = 10^{-8.82} M_{\odot} \text{ yr}^{-1}$. Curve designations are the same as in Fig. 5a. Maximum values of the quantities shown are $\tau_{\text{mid}} = 13.7$, $\Sigma = 74.7 \text{ g cm}^{-2}$, $F_s = 4.18 \times 10^{10} \text{ ergs cm}^{-2} \text{ s}^{-1}$, $T_{\text{mid}} = 7040 \text{ K}$ ($T_s = 4588 \text{ K}$), $P_{\text{mid}} = 3.83 \times 10^4 \text{ dyn cm}^{-2}$, and $\rho_{\text{mid}} = 8.50 \times 10^{-8} \text{ g cm}^{-3}$. There is only weak convection occurring, although it extends over 57% (in Σ) of the structure. (b) Vertical structure of a Σ_{\max} solution; $\alpha = 0.01$, $r = 10^{10.5}$ cm, and $\dot{M} = 10^{-8.80} M_{\odot} \text{ yr}^{-1}$. Curve designations are the same as in Fig. 5a. Maximum values of the quantities shown are $\tau_{\text{mid}} = 1.76 \times 10^6$, $\Sigma = 1910 \text{ g cm}^{-2}$, $F_s = 4.38 \times 10^{10} \text{ ergs cm}^{-2} \text{ s}^{-1}$, $T_{\text{mid}} = 18,510 \text{ K}$ ($T_s = 4641 \text{ K}$), $P_{\text{mid}} = 1.99 \times 10^6 \text{ dyn cm}^{-2}$, and $\rho_{\text{mid}} = 9.80 \times 10^{-7} \text{ g cm}^{-3}$. The structure is again dominated by convection. Minimum value of $F_{\text{rad}}/F_{\text{tot}}$ is 4.22×10^{-5} .

more severe than for the solution with $\alpha = 0.01$. The structure for $\alpha = 1.0$ also has a larger core of inefficient convection. This is because the convective flux increases with density, whereas the radiative flux decreases. The higher density at lower α thus increases the convective efficiency.

The photosphere occurs where $T \approx 1.14 T_s$, T_s being the temperature in the top of the disk. Note that the disk becomes isothermal in the outermost part because of the very small densities. The disk optical depth is far larger than predicted by the diffusion equation $T_{\text{mid}}^4 \approx \tau_{\text{mid}} T_{\text{eff}}^4$ because of convection. All solutions with $T_{\text{mid}} \approx 10,000$ – $20,000 \text{ K}$ and $T_{\text{eff}} \approx 5000 \text{ K}$ show this same gross structure.

Figures 9a and 9b present the vertical structure at the local maximum in Σ with respect to T_{eff} , Σ_{\max} , for $r = 3 \times 10^{10}$ cm and for $\alpha = 1.0$ and 0.01 , respectively. These figures illustrate the dramatic difference in structure at Σ_{\max} between large and small α . The solution for $\alpha = 0.01$ has a density inversion near the midplane and a smaller one near the photosphere, as for the solution for $\alpha = 0.01$ of Figure 8b. For $\alpha = 1.0$, convection carries a small part of the flux, although it extends over 57% of the structure as measured by the surface density. This is because the opacity is small at $T_{\text{mid}} = 7040 \text{ K}$. The $\alpha = 0.01$ solution has $T_{\text{mid}} = 18,510 \text{ K}$. Convection carries all but 10^{-4} of the flux at the point of greatest convective efficiency.

Table 2 gives some of the physical conditions at points of $\Sigma_{\max} = \max(\Sigma_{\max,1}, \Sigma_{\max,2})$ in this partial ionization regime. Figure 10 presents the dependence of Σ_{\max} on r and α . These critical points were determined to 0.01 dex in \dot{M} . For $\alpha \geq 0.3$ the maximum caused by the opacity decrease is at larger Σ and for smaller α the convective maximum is at larger Σ .

Figure 11 shows in more detail the manner in which the locations of the maxima in surface density depend on α . For $\alpha = 1$ the effect of the opacity decrease is dominant. As one approaches this inflection point from higher temperatures the midplane temperature drops below 10^4 K . From Table 2 the midplane temperature at the maximum in surface density can range from 6500 to 7700 K depending on r . For $\alpha = 0.3$ three peaks are evident, and the surface density associated with the opacity decrease is slightly larger than that induced by convection. For $\alpha = 0.1$ the surface density maximum associated with the opacity decrease ($\Sigma_{\max,1}$) is less than that associated with convection ($\Sigma_{\max,2}$). The third peak, which is only evident in the curve for $\alpha = 0.3$ in Figure 11, is caused by a combination of two effects. The opacity at the midplane begins to decrease less rapidly with temperature because of absorption by H_2O and TiO , and the optical depth is small, so the term $1 - e^{-2\tau_{\text{mid}}}$ has some effect on the structure. We do not know specifically how this combined effect of opacity and optical depth causes this bump. This peak is not evident in the curve for $\alpha = 1.0$ because the midplane temperature never gets small enough. It does not appear in the curves for smaller α because the optical depth is too high.

For $\alpha < 0.1$ the effect of the opacity peak is merely to cause a change in slope in Figure 11, and the effect of convection is entirely responsible for the maximum in surface density. Apparently, MM2 did not explicitly study the maximum induced by the rapid decrease of opacity ($\Sigma_{\max,1}$) because they only considered $\alpha = 0.07$ and 0.02 . For these values the effect of the opacity per se is only a very minor feature compared to the principal maximum in surface density induced by convection.

TABLE 2
 CONDITIONS AT LOCAL MAXIMA OF SURFACE DENSITY WITH RESPECT TO T_{eff}

$\log r(\text{cm})$	$-\log \alpha$	$-\log \dot{M}(M_{\odot} \text{ yr}^{-1})$	Σ (g cm^{-2})	T_{mid} (K)	T_{eff} (K)	τ_{mid}	h/r ($\rho/\rho_{\text{mid}}=1\%$)
11.50	2.0	6.32	21440.	16980	4011	1.03+7	0.141
	1.5	6.29	8190.	17450	4082	1.93+6	0.127
	1.0	6.26	3232.	18210	4153	3.40+5	0.114
	0.5	6.70	1379.	6571	3223	82.7	0.0620
	0.0	6.39	840.2	6468	3853	36.0	0.0724
11.00	2.0	7.52	6419.	18960	4729	4.30+6	0.0851
	1.5	7.53	2462.	18210	4702	8.33+5	0.0736
	1.0	7.61	985.8	15900	4490	1.03+5	0.0603
	0.5	7.90	443.5	6794	3800	49.1	0.0377
	0.0	7.60	250.8	6901	4516	25.9	0.0460
10.50	2.0	8.80	1906.	18510	5286	1.76+6	0.0465
	1.5	8.79	733.4	18090	5317	3.36+5	0.0414
	1.0	8.84	298.2	16260	5166	4.48+4	0.0351
	0.5	9.10	133.2	6793	4448	23.2	0.0256
	0.0	8.82	74.74	7040	5226	13.7	0.0277
10.00	2.0	10.07	546.6	18250	5858	6.41+5	0.0256
	1.5	10.07	210.8	17360	5858	1.16+5	0.0227
	1.0	10.06	86.61	16580	5892	1.86+4	0.0204
	0.5	10.28	39.84	7396	5191	18.7	0.0155
	0.0	10.03	20.97	7528	5994	9.85	0.0166
9.5	2.0	11.27	152.8	18530	6534	2.31+5	0.0144
	1.5	11.27	59.11	17440	6534	4.13+4	0.0128
	1.0	11.29	24.12	15920	6459	5.42+3	0.0114
	0.5	11.43	11.48	7525	5959	9.53	9.30-3
	0.0	11.21	5.63	7674	6764	4.91	9.55-3

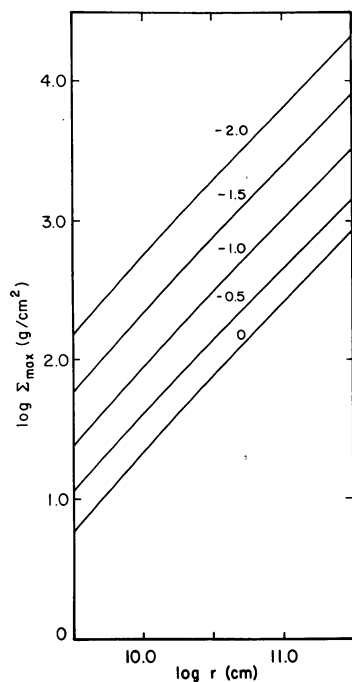


FIG. 10.—Values of Σ_{max} as a function of r for varying α . The scaling with α changes slightly for $\alpha \geq 0.3$, while the vertical structure associated with Σ_{max} changes drastically.

Recently Mineshige and Osaki (1983) have independently discovered these two Σ inversion features associated with steady-state solutions. They use $\alpha = 0.1$ and $\alpha = 0.032$ and yet a third mixing-length prescription different from either that employed here or by MM2. They too find that $\Sigma_{\text{max},2} > \Sigma_{\text{max},1}$ for these small α .

The relative ordering of the effect of the opacity decrease and convection with α holds true for all radii. This is true because convective flux is proportional to density and radiative flux is inversely proportional to density (see eq. [3]). Since lower α solutions have larger densities, convection becomes more important in carrying the flux and determining the vertical structure. Although convection carries most of the flux over much of the vertical structure of the solution depicted in Figure 8a for which $\alpha = 1.0$, it does not lower the temperature gradient sufficiently to bring about a Σ reversal in that region of parameter space.

As stated earlier, CGW assumed an adiabatic vertical structure for regions which were convectively unstable. As Mineshige and Osaki (1983) note, this corresponds to mixing-length convection with $l = \infty$. In stellar interiors this is often a good approximation, but for the solutions encountered here $\rho \approx 10^{-8} \text{ g cm}^{-3}$, so this assumption is questionable, and we have incorporated the effects of a mixing-length theory of convection. With MLT we find ∇ exceeds ∇_{ad} by as much as 10^2 – 10^3 in convective regions near the midplane. Near the

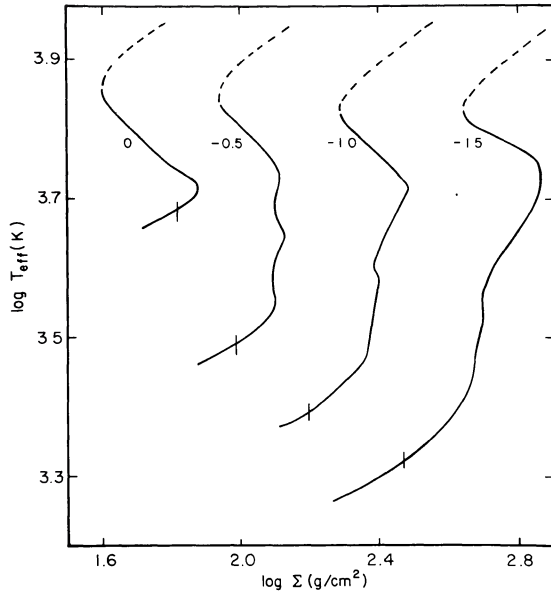


FIG. 11.—Curves of constant r and α and varying \dot{M} for four values of α . Small numbers to the left of the curves are $\log \alpha$; $r = 10^{10.5}$ cm for all four curves. Vertical bars show where the first midplane convection appears as one ascends the curves. Full disk optical depth at these points is ~ 3 . For $\alpha < 0.3$, $T_{\text{mid}}(\Sigma_{\text{max}}) \approx 17,000$ K, and the vertical structure is very convective. For $\alpha = 0.3$ the $T_{\text{mid}} \approx 7000$ K peak is slightly larger than the $T_{\text{mid}} \approx 17,000$ K peak. The $T_{\text{mid}} \approx 7000$ K peak has negligible convection. There is a third peak for this α at $\log T_{\text{eff}} = 3.5$ because of TiO and H₂O. For $\alpha = 1.0$ only the $T_{\text{mid}} \approx 7000$ K peak is evident. At slightly cooler temperatures convection goes away, and just below that the solutions become optically thin. The relative ordering of these peaks does not depend on r .

midplane the gravity and the temperature gradient decrease, and the convection is very inefficient. Away from the midplane the radiative gradient drops off rapidly to a value just a little in excess of the adiabatic gradient, and convection carries a major portion of the flux. Thus, portions of the convective regions can be very inefficient by stellar interior standards.

If convection dominates the maximum in Σ (i.e., small α) the maximum occurs when the midplane temperature is very near the peak in the Rosseland opacity curve for that midplane density. This is true regardless of the convection theory used and comes about because these solutions with the largest opacity and, hence, radiative gradient are most strongly affected by convection. Since MLT convection has a steeper temperature gradient, it will have a smaller effective temperature for the same midplane temperature, α , and r than adiabatic convection. This means that the effective temperature corresponding to Σ_{max} will be smaller for inefficient MLT than for adiabatic convection.

Using the adiabatic assumption $\nabla = \nabla_{\text{ad}}$, we find the loci of maximum Σ is given roughly by

$$T_{\text{mid,max}} \approx 13,550 \text{ K } \alpha^{-0.1}, \quad (23)$$

and

$$\Sigma_{\text{max}} = 47.1 \text{ g cm}^{-2} \alpha^{-0.85} r_{10}^{1.31}. \quad (24)$$

The effective temperature of this point is relatively insensitive to r and α :

$$T_{\text{eff,max}} = 9500 \text{ K } r_{10}^{-\epsilon_1} \alpha^{\epsilon_2}, \quad (25)$$

where $\epsilon_1 \approx 0.04$ and $\epsilon_2 < 0.01$. For this convection $\Sigma_{\text{max}} = \Sigma_{\text{max,2}}$ for all α . The hydrogen recombination feature $\Sigma_{\text{max,1}}$ is a very minor effect. Using the mixing-length theory of convection described in Schwarzschild (1958), we find

$$T_{\text{mid,max,2}} \approx 15100 \text{ K } \alpha^{-0.04}, \quad (26)$$

$$\Sigma_{\text{max,2}} = 15.2 \text{ g cm}^{-2} \alpha^{-0.80} r_{10}^{1.06}, \quad (27)$$

and $T_{\text{eff}} \approx 5300 \text{ K } r_{10}^{0.1}$, quite different from the adiabatic models. This shows, unfortunately, that the results are sensitive to the treatment of convection, or more specifically, the value of the mixing length used. For the hydrogen recombination feature we find

$$\Sigma_{\text{max,1}} \approx 22 \text{ g cm}^{-2} \alpha^{-0.5} r_{10}^{1.05}, \quad (28)$$

and

$$T_{\text{mid,max,1}} \approx 7000 \text{ K}. \quad (29)$$

Although the scaling for Σ_{max} is not given explicitly in MM2, it can be taken from their plotted results to be approximately

$$\Sigma_{\text{max}} = 12.6 \text{ g cm}^{-2} \alpha^{-0.83} r_{10}^{1.11}, \quad (30)$$

very close to our results. They also find $T_{\text{mid,max}} \approx 16,000$ K for $\alpha = 0.07$ independent of r , again in quantitative agreement with the present results. Their value of $T_{\text{eff,max}} = 6500$ K is somewhat above ours. This Σ_{max} corresponds to $\Sigma_{\text{max,2}}$, the convective feature. As mentioned above, they do not find $\Sigma_{\text{max,1}}$ since only a small α is used.

If one changes the mixing length drastically, the portions of the structure where convection is important are moved to different surface density. We recomputed several steady-state solutions using $l^* = 1/3$ and $3/2$ [$l^* = l/\min(z, H_p)$]. For example, for $l^* = 1/3$, the reduced convective efficiency causes the midplane temperature to rise and the surface density to decrease for given r , \dot{M} , and α compared to the present solutions. The surface density maximum $\Sigma_{\text{max}} = \max(\Sigma_{\text{max,1}}, \Sigma_{\text{max,2}})$ is larger by a factor of ~ 2 for $\alpha \approx 0.01$ and by a few percent for $\alpha \approx 1$. An increase in the mixing length causes the point representing Σ_{max} to correspond to a larger rate of accretion. For example, for $l^* = 1.5$, T_{eff} is $\sim 15\%$ higher and $\Sigma \sim 10\%$ larger than when $l^* = 1$ is used. As l^* increases, convection becomes more efficient, and the temperature gradient is reduced. This reduces T_{mid} and raises Σ . Hence, the fact that $\Sigma_{\text{max,2}} > \Sigma_{\text{max,1}}$ for $\alpha < 0.3$ and $\Sigma_{\text{max,2}} < \Sigma_{\text{max,1}}$ for $\alpha \geq 0.3$ is a direct result of using $l^* = 1$. If l^* were smaller than some critical value l_1^* , one would find that $\Sigma_{\text{max,1}}$ would be larger for all α , and if l^* were larger than some critical value l_2^* , then $\Sigma_{\text{max,2}}$ would be dominant. Since convection is so unimportant for solutions with $T_{\text{mid}} \approx 7000$ K, $\Sigma_{\text{max,1}}$ is insensitive to the value of l^* . Only $\Sigma_{\text{max,2}}$ is affected—and more so for smaller α .

The fact that the present results for $\alpha = 0.1$ agree so well with those of MM2 and Mineshige and Osaki (1983), all of whom use slightly different theories of convection, suggests that the value of the mixing length l is much more important in setting the disk structure than the mixing theory used. Hence, although the Schwarzschild treatment ignores the radiative losses of the convective elements and the Böhm-Vitense treatment considers this effect, the disk is sufficiently thin that the elements only move a short distance in their lifetime in either event. A determination of l_1^* and l_2^* would require considerably more effort and is beyond the scope of this work. These quantities are probably roughly $1/2$ and 2 , respectively. Mineshige and Osaki (1983) examine how $\Sigma_{\max,2}$ depends on l^* for $\alpha = 0.1$ by computing tracks for $l^* = 0.7, 1.0$, and 2.0 . For $l^* = 0.7$ they find $\Sigma_{\max,2} \approx \Sigma_{\max,1}$. For $l^* = 2.0$ they start to recover the solutions of CGW, for which $l^* = \infty$.

One important difference between the maximum in surface density induced by the opacity decrease and that induced by convection is that the viscous time scale at Σ_{\max} is considerably different for the two effects. The viscous time scale is proportional to $\mu_{\text{mid}}/T_{\text{mid}}$. For the convective maximum $T_{\text{mid}} \approx 17,000$ K and $\mu_{\text{mid}} \approx 0.65$, while for the opacity maximum $T_{\text{mid}} \approx 7000$ K and $\mu_{\text{mid}} \approx 1.3$. Thus, the viscous time scale is ~ 4 times larger for the latter peak for comparable α . This will effect the rate at which material accumulates to a critical surface density, and the time between bursts.

iv) Radiative Solutions

When the midplane temperature is $\sim 20,000$ – $40,000$ K (depending on α), a local minimum in Σ occurs. In the limit cycle model of MM1 this is the feature which causes the disk to go from a high to low viscosity state as $\Sigma(r)$ decreases below the minimum critical value. At these minima, convection just barely extends down to the midplane. For higher \dot{M} , convection is only present in layers of partially ionized hydrogen and helium above the midplane. Our results for Σ_{\min} agree very closely with those of MM2. We find

$$\Sigma_{\min} \approx 191 \text{ g cm}^{-2} r_{10.5}^{1.11} \alpha^{-0.70}, \quad (31)$$

whereas MM2 find

$$\Sigma_{\min} \approx 162 \text{ g cm}^{-2} r_{10.5}^{1.11} \alpha^{-0.80}. \quad (32)$$

Also we get

$$T_{\text{mid,min}} \approx 39,000 \text{ K } r_{10.5}^{\epsilon} \alpha^{-0.2}, \quad (33)$$

where ϵ is several hundredths. The scaling of Σ_{\min} with r and α is shown in Figure 12 and given in Table 3.

Figures 13a and 13b show the vertical structure at Σ_{\min} for $r = 10^{10.5}$ cm and $\alpha = 1.0$ and 0.01 , respectively. These solutions have higher midplane temperatures than vertical structures depicted in the previous structure graphs but still have $T_{\text{eff}} < 10^4$ K, so some portion of the vertical structure must correspond to the peak in the opacity. The density inversion caused by "opacity peak" convection is a localized bump near the disk surface, and the flux carried by convection at that

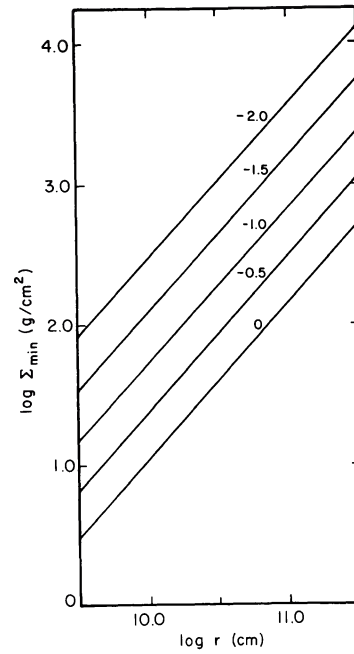


FIG. 12.—Values of Σ_{\min} as a function of r for varying α . These are given quite accurately by power-law scalings.

point is much smaller than in the Σ_{\max} solutions. The $\alpha = 0.01$ solution has, in addition, a region at smaller z where convection is induced by partially second-ionized helium. This is not found in the $\alpha = 1.0$ structure because it is at a much lower temperature.

At hotter temperatures there is no midplane convection. The solutions obtained are close to a power law scaling

$$\Sigma = 2240 \text{ g cm}^{-2} \alpha^{-0.81} \dot{M}_{-6}^{0.66} r_{10}^{-0.66}. \quad (34)$$

The vertically averaged approach of Shakura and Sunyaev (1973) gives

$$\Sigma = 6560 \text{ g cm}^{-2} \alpha^{-0.80} \dot{M}_{-6}^{0.70} r_{10}^{-0.75} \quad (35)$$

for $P = P_g$, $\kappa = \kappa_{\text{ff}}$, and

$$\Sigma = 5210 \text{ g cm}^{-2} \alpha^{-0.80} \dot{M}_{-6}^{0.60} r_{10}^{-0.60} \quad (36)$$

for $P = P_g$, $\kappa = \kappa_{\text{es}}$. The vertically integrated solutions contain a mixture of free-free "like" opacity and electron scattering, so it is not surprising that the functional dependencies in our equation lie between these two extremes. Our scaling for midplane temperature is

$$452,000 \text{ K } \alpha^{-0.20} \dot{M}_{-6}^{0.30} r_{10}^{-0.72}, \quad (37)$$

while SS give for gas pressure and free-free opacity

$$228,000 \text{ K } \alpha^{-0.20} \dot{M}_{-6}^{0.30} r_{10}^{-0.75}, \quad (38)$$

and for electron scattering

$$288,000 \text{ K } \alpha^{-0.20} \dot{M}_{-6}^{0.40} r_{10}^{-0.90}. \quad (39)$$

TABLE 3
CONDITIONS AT LOCAL MINIMA OF SURFACE DENSITY WITH RESPECT TO T_{eff}

$\log r$ (cm)	$-\log \alpha$	$-\log \dot{M} (M_{\odot} \text{ yr}^{-1})$	Σ (g cm^{-2})	T_{mid} (K)	T_{eff} (K)	τ_{mid}	h/r ($\rho/\rho_{\text{mid}} = 1\%$)
11.5	2.0	5.77	13100.	69020	5506	9.82+4	0.302
	1.5	5.78	5443.	53740	5474	5.00+4	0.246
	1.0	5.75	2350.	43580	5569	1.77+4	0.209
	0.5	5.72	1085.	34270	5666	7.75+3	0.174
	0.0	5.65	514.7	28080	5900	2.88+3	0.154
11.0	2.0	7.07	3777.	66730	6128	5.11+4	0.167
	1.5	7.07	1573.	52670	6128	2.36+4	0.138
	1.0	7.06	681.6	41660	6163	9.22+3	0.114
	0.5	7.02	310.6	32780	6306	3.34+3	0.0985
	0.0	6.96	144.8	26640	6527	1.22+3	0.0871
10.5	2.0	8.38	1059.	62910	6732	2.86+4	0.0904
	1.5	8.39	438.1	49630	6694	1.29+4	0.0740
	1.0	8.37	191.3	39210	6771	4.61+3	0.0629
	0.5	8.33	86.46	30740	6928	1.59+3	0.0547
	0.0	8.28	39.71	24970	7131	5.56+2	0.0484
10.0	2.0	9.67	291.5	59320	7375	1.51+4	0.0494
	1.5	9.67	121.2	47440	7375	6.04+3	0.0412
	1.0	9.66	52.87	36570	7417	2.27+3	0.0346
	0.5	9.63	23.71	28630	7547	8.23+2	0.0299
	0.0	9.58	10.84	10.84	23340	7767	2.62+2
9.5	2.0	10.90	80.15	56330	8085	7.88+3	0.0269
	1.5	10.90	33.76	44470	8085	3.13+3	0.0225
	1.0	10.88	14.68	34380	8179	1.08+3	0.0194
	0.5	10.85	6.54	27140	8321	3.88+2	0.0169
	0.0	10.79	3.00	3.00	22340	8614	1.27+2

The different numerical coefficients between our formulae (eqs. [34], [37]) and those of SS (eqs. [35], [36], [38], [39]) comes from using realistic values of mean molecular weight and opacity.

Figures 14a and 14b present radiative vertical structure solutions at $r = 3 \times 10^{10}$ cm for $\alpha = 1.0$ and 0.01, respectively. Note that the ratio of midplane to surface temperature is much larger than for previous vertical structure plots. Convection carries a small amount of the flux at $z = 2.3 \times 10^9$ cm in the $\alpha = 1.0$ solution.

Equation (34) gives radiative curves which are quite close to those presented graphically by MM2. This equation begins to fail when the midplane temperature becomes too large. Then radiation pressure starts to contribute more to the total pressure, and so curves of constant r and α in the $\log T_{\text{eff}} - \log \Sigma$ plane have increasingly large slope which tends to ∞ as they approach the LE unstable regime. Setting the viscous stress tensor proportional to gas pressure instead of total pressure avoids this situation. It is not known whether it is more physical to take $t_{\phi r} = \alpha P_{\text{tot}}$ or αP_{gas} .

IV. DISCUSSION

Osaki (1974) proposed that the optical bursts seen in dwarf novae may be caused by a ringlike structure of low-viscosity material formed from the Roche lobe overflow of the secondary which piles up around the white dwarf. Hoshi (1979) was the first to investigate the physical basis of this proposal.

After some critical mass is stored, an instability is presumed to develop, and the accumulated material goes to a state of higher viscosity and much faster evolution time. The burst is caused by a rapid dumping of this gas onto the white dwarf and release of its gravitational energy. The two-dimensional calculations of Hensler (1982b) mentioned above support this idea. His low-viscosity run with the parameters relevant to a "disk in quiescence" shows a ringlike build up of material at roughly the injection radius (see model 3, Fig. 6, p. 325). Such a feature also shows up in the time-dependent models of PFL and Smak (1983a). The word "ring" is taken here and below to mean a structure which has $\Sigma(r)$ less than some $\Sigma_{\text{crit}}(r)$ for all r , as opposed to a standard "disk" which has a surface density maximum at small r which greatly exceeds Σ_{crit} . Most of a "disk" is hence by definition in a bursting state. Regardless of which instability is invoked, Σ_{crit} is roughly proportional to radius.

MM1 suggested the $\Sigma_{\text{max},2}$ feature as the specific instability mechanism, while CGW suggested the transition between nonconvective and convective solutions at $T \approx 2500$ K as the cause. Constraints on either model can, in principle, be set without a complete time-dependent calculation by examining the fundamental time scales. Two basic observational time scales are the time between bursts (t_{twixt}) and the length of the burst (t_{burst}). The rise time provides another independent constraint, but the physics of it is very model dependent, and we have not found a satisfactory semianalytic description of it even in the context of our favored model which starts from a

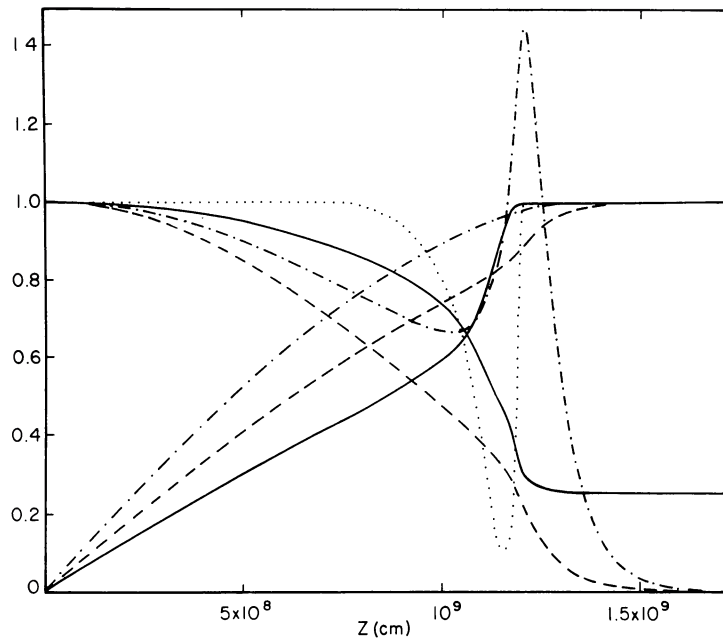


FIG. 13a

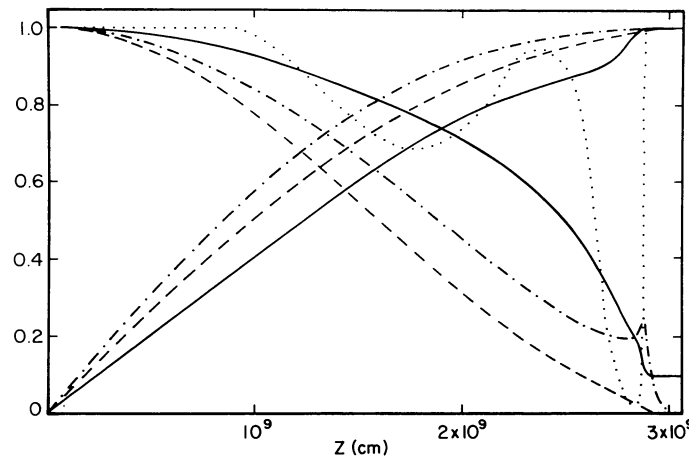


FIG. 13b

FIG. 13.—(a) Vertical structure of a Σ_{\min} solution; $\alpha=1.0$, $r=10^{10.5}$ cm, and $\dot{M}=10^{-8.28} M_{\odot} \text{ yr}^{-1}$. Curve designations are the same as in Fig. 5a. Maximum values of the quantities shown are $\tau_{\text{mid}}=556$, $\Sigma=39.7 \text{ g cm}^{-2}$, $F_s=1.45 \times 10^{11} \text{ ergs cm}^{-2} \text{ s}^{-1}$, $T_{\text{mid}}=24,970 \text{ K}$ ($T_s=6261 \text{ K}$), $P_{\text{mid}}=5.41 \times 10^4 \text{ dyn cm}^{-2}$, and $\rho_{\text{mid}}=1.67 \times 10^{-8} \text{ g cm}^{-3}$. The structure shows “opacity peak” convection caused by partially ionized hydrogen. This inefficient convection produces a superadiabatic temperature gradient and a density inversion. Minimum value of $F_{\text{rad}}/F_{\text{tot}}$ is 0.10. (b) Vertical structure of a Σ_{\min} solution; $\alpha=0.01$, $r=10^{10.5}$ K, and $\dot{M}=10^{-8.38} M_{\odot} \text{ yr}^{-1}$. Curve designations are the same as in Fig. 5a. Maximum values of the quantities shown are $\tau_{\text{mid}}=2.86 \times 10^4$, $\Sigma=1060 \text{ g cm}^{-2}$, $F_s=1.15 \times 10^{11} \text{ ergs cm}^{-2} \text{ s}^{-1}$, $T_{\text{mid}}=62,910 \text{ K}$ ($T_s=5911 \text{ K}$), $P_{\text{mid}}=2.41 \times 10^6 \text{ dyn cm}^{-2}$, and $\rho_{\text{mid}}=2.83 \times 10^{-7} \text{ g cm}^{-3}$. The “opacity peak” convection at $z \approx 2.7 \times 10^9$ cm induces a small density inversion, while the less efficient $\text{He}^{++}\text{-He}^{++}$ convection at $z \approx 1.7 \times 10^9$ cm does not. The previous Σ_{\min} solution (for $\alpha=1.0$) did not show $\text{He}^{++}\text{-He}^{++}$ convection because its midplane temperature was below that needed to ionize He^+ . Minimum value of $F_{\text{rad}}/F_{\text{tot}}$ is 0.020.

well-defined ring. We do not address it here except in a general way. There are three relevant physical time scales, the time to build to a critical surface density in the vicinity of the injection radius (t_{store}), the time for the cold ring to spread through an appreciable range in radius (t_{spread}), and the duration of the bursts (t_{burst}). In the context of models in which a well-defined ring grows to critical density at the point of mass input (i.e., that of CGW), t_{store} represents the time

between bursts, t_{twixt} . For these models, the time scales set two boundaries on the transfer rate and the radius of the ring, as discussed in CGW and Cannizzo, Wheeler, and Ghosh (1983). One of these constraints is $t_{\text{burst}} < t_{\text{store}}$. If this constraint is violated, the burst lasts longer than the time to reach a critical state; that is, steady-state accretion occurs. Another bound is $t_{\text{store}} < t_{\text{spread}}$. This is not a firm physical boundary, but a bound on this class of models (a point not appreciated at the

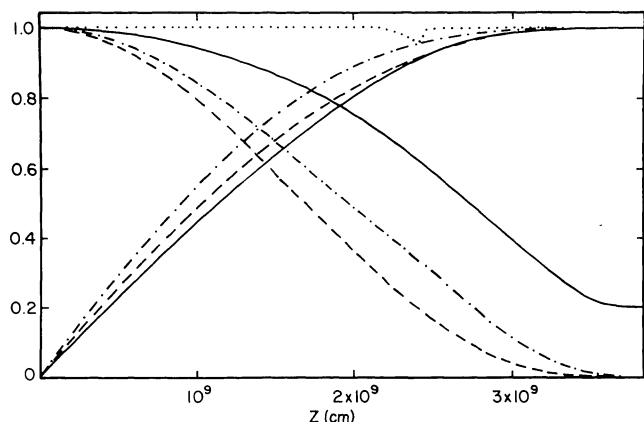


FIG. 14a

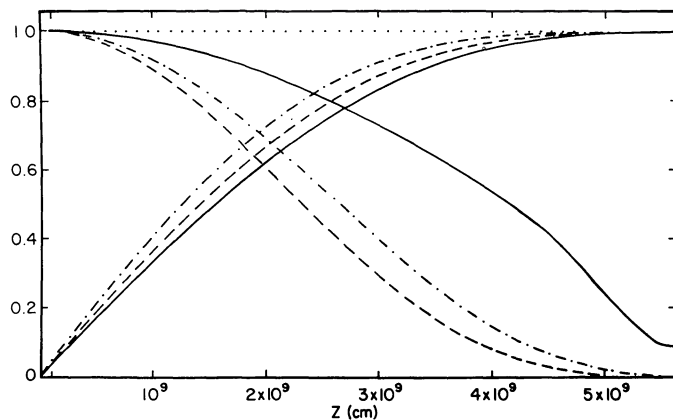


FIG. 14b

FIG. 14.—(a) Vertical structure of a hot radiative solution; $\alpha=1.0$, $r=10^{10.5}$ cm, and $\dot{M}=10^{-7.00} M_{\odot} \text{ yr}^{-1}$. Curve designations are the same as in Fig. 5a. Maximum values of the quantities shown are $\tau_{\text{mid}}=806$, $\Sigma=222 \text{ g cm}^{-2}$, $F_s=2.76 \times 10^{12} \text{ ergs cm}^{-2} \text{ s}^{-1}$, $T_{\text{mid}}=64,670 \text{ K}$ ($T_s=13,080 \text{ K}$), $P_{\text{mid}}=4.93 \times 10^5 \text{ dyn cm}^{-2}$, and $\rho_{\text{mid}}=5.72 \times 10^{-8} \text{ g cm}^{-3}$. Ratio of gas pressure to total pressure at the midplane is 0.918. This solution is radiative everywhere, except for a small amount of convection due to partially ionized He^+ at $z=2.3 \times 10^9$ cm. (b) Vertical structure of a hot radiative solution; $\alpha=0.01$, $r=10^{10.5}$ cm, and $\dot{M}=10^{-7.30} M_{\odot} \text{ yr}^{-1}$. Curve designations are the same as in Fig. 5a. Maximum values of the quantities shown are $\tau_{\text{mid}}=2.60 \times 10^4$, $\Sigma=5730 \text{ g cm}^{-2}$, $F_s=1.38 \times 10^{12} \text{ ergs cm}^{-2} \text{ s}^{-1}$, $T_{\text{mid}}=129,300 \text{ K}$ ($T_s=11,010 \text{ K}$), $P_{\text{mid}}=1.93 \times 10^7 \text{ dyn cm}^{-2}$, and $\rho_{\text{mid}}=1.08 \times 10^{-6} \text{ g cm}^{-3}$. Ratio of gas pressure to total pressure at the midplane is 0.963. This solution is radiative, except for a small amount of convection due to partially ionized He^+ at $z=4.5 \times 10^9$ cm.

time of writing of CGW and Cannizzo, Wheeler, and Ghosh 1983). If this boundary is violated, the material will spread inward, and the instability will be triggered at a smaller radius where the surface density is not, in general, a global maximum. For such a case the time scale t_{spread} sets the time between bursts, t_{wixt} . This class of models is that implied by MM1, MM2 and explored in some detail by PFL. We discuss below the manner in which a comparison of the observational and physical time scales sets limits on the two classes of models. From these limits, one can, in principle, place bounds on the location of the quiescent ring (r_{ring}) and, hence, on the amount of material stored and on the burst luminosity.

We have approximated t_{spread} and t_{burst} with preliminary results obtained from time-dependent work. We used the method described in Bath and Pringle (1981) which combines the equations of conservation of mass and angular momentum in the \hat{r} direction with the vertically averaged treatment. We followed the viscous evolution of rings of material initially placed at $r_{\text{ring}}=10^{10.5}$ cm around a $1 M_{\odot}$ object. These rings were given Gaussian profiles of surface density peaked at r_{ring} with varying half-widths $\delta r_{\text{initial}}=f \times r_{\text{ring}}$ and maxima $\Sigma_{\text{peak,initial}}$. These runs were confined to “radiative solutions” described in § IIIbiv which are characteristic of the outburst disk. We used $\alpha=1$. After the runs start, the rings spread out and accrete onto the central object. The maximum value of the surface density decreases during the initial spreading and then increases as the bulk of the ring moves to small r . A quasi-steady-state disk is established with a density profile approximating that given by SS for the “outer region”: $\Sigma \propto r^{-3/4} [1 - \sqrt{(r_{\text{wd}}/r)}]^{0.7}$. The rate of accretion at the inner edge of the disk is very high, and the collected ring material drains out of the disk during the subsequent evolution.

For our purposes we have extracted approximations for two time scales. These are the time t_{spread} for Σ_{peak} to go through a minimum during the initial spreading, and the one e -fold

decay time t_{fall} for the bolometric luminosity, starting from the time when L_{disk} peaks. This latter phase occurs when the stored material is being accreted.

One might expect one or both of these viscous time scales to behave like $t_{\text{ss}} = \Delta M / \dot{M}(\Delta M)$, where $\dot{M}(\Delta M)$ is the rate of accretion in a steady-state accretion disk with a mass equal to that in an initial ring of mass ΔM . If one takes $\Sigma = \Sigma_0 r^a \alpha^b \dot{M}^c$, then a simple integration over the disk gives

$$t_{\text{ss}} = [2\pi \Sigma_0 / (2+a)]^{1/c} \alpha^{b/c} \Delta M^{(1-1/c)} r_{\text{out}}^{(2+a)/c}, \quad (40)$$

where r_{out} is the outer edge of the disk. A steady-state model calculated with the vertically averaged time-dependent treatment gives $a=-0.75$, $b=-0.8$, and $c=0.7$; hence, $t_{\text{ss}} \propto \Delta M^{-0.43}$. We find for the calculation of the spreading torus

$$t_{\text{spread}} \approx 200 \text{ min} \left(\Sigma_{\text{peak,init}} / 600 \text{ g cm}^{-2} f / 0.3 \right)^{-0.42}, \quad (41)$$

and

$$t_{\text{fall}} \approx 2000 \text{ min} \left(\Sigma_{\text{peak,init}} / 600 \text{ g cm}^{-2} \right)^{-0.37} (f / 0.3)^{-0.3}, \quad (42)$$

where these scalings apply for $\Sigma_{\text{peak,init}} \approx 600 \text{ g cm}^{-2}$ and aspect ratio $f \approx 0.3$. We ignore the α dependency of f . From equation (40) one would expect the time scales to go as $(\Sigma f)^{(1-1/c)} = (\Sigma f)^{-0.43}$. Thus, we see that equation (40) provides a reasonable representation of the spreading time scale. That the magnitudes of the exponents of Σ and f in the expression for t_{fall} are less than 0.43 seems to indicate that r_{out} goes as some small positive power of these quantities. We initially expected that the time for the ring to spread in surface area would also represent the rise time to peak

luminosity, but our numerical models give rather different scalings (i.e., not a simple function of ΔM). We do not yet understand the factors determining the rise time in this class of models.

To describe the spreading of material in the cold, quiescent state, the time scale in equation (41) must be scaled to appropriate conditions. This is done in the following way. The classical disk drift time t_{drift} is given by

$$t_{\text{drift}} = 2\pi r^2 \Sigma / \dot{M} = 2.4 \text{ weeks } \mu_{\text{mid}} r_{10}^{0.5} / \alpha T_{\text{mid},4} \propto (\mu / \alpha T)_{\text{mid}}. \quad (43)$$

Hence, the numerical coefficient of t_{spread} is scaled by the value of $(\mu / \alpha T)_{\text{mid}}$ for the quiescent ring being considered. The coefficient of equation (41) is for the parameters $\alpha \approx 1.0$, $T_{\text{mid}} \approx 10^5$ K, and $\mu_{\text{mid}} \approx 0.65$. The conditions for the CGW model are $\alpha \approx 0.01$, $T_{\text{mid}} \approx 2000$ K, and $\mu_{\text{mid}} \approx 2.4$. For the MM model: $\alpha \approx 0.1$, $T_{\text{mid}} \approx 17,000$ K, and $\mu_{\text{mid}} \approx 0.65$ for $\alpha < 0.3$; $\alpha \approx 1.0$, $T_{\text{mid}} \approx 7000$ K, and $\mu_{\text{mid}} \approx 1.3$ for $\alpha \geq 0.3$. For Σ the value for either $\Sigma_{\text{conv}}(\text{CW})$ or $\Sigma_{\text{max}}(\text{MM})$ is used. This is admittedly crude because it assumes the ring is in its critical state all through quiescence. In reality, the ring starts at some lower temperature and viscosity and builds up to this state as more material is deposited. This scaling also neglects the fact that if the material is optically thin in quiescence, the evolution time is increased. Hence, the expression used for t_{drift} is an underestimate. Also, even though we have used time-dependent results to adjust the numerical coefficients on the time scales, they are still only approximations to complicated time-dependent phenomena. These approximations are no substitute for a complete time-dependent study, but they do give some feel for the behavior of the models and do illustrate some of the qualitative differences between the different classes of models.

We now take the spreading time from equation (41), with the coefficient modified as just discussed, $t_{\text{burst}} = 3t_{\text{fall}}$ using equation (42), and

$$t_{\text{store}} = 2\pi r^2 f \Sigma_{\text{crit}} / \dot{M}_T. \quad (44)$$

We rewrite the Σ_{crit} values for $r = 10^{10.5}$ cm as

$$\Sigma(\text{CW}) = 533 \text{ g cm}^{-2} \alpha_{-2}^{-0.49} r_{10.5}^{0.76}, \quad (45)$$

$$\Sigma(\text{MM}, \alpha \geq 0.3) = 74.8 \text{ g cm}^{-2} \alpha^{-0.5} r_{10.5}^{1.05}, \quad (46)$$

and

$$\Sigma(\text{MM}, \alpha < 0.3) = 1900 \text{ g cm}^{-2} \alpha_{-2}^{-0.8} r_{10.5}^{1.06}. \quad (47)$$

The luminosity is taken to be

$$L = 1/2 GM_{\text{wd}} \dot{M}_T / r_{\text{wd}} \min(t_{\text{spread}}, t_{\text{store}}) / t_{\text{burst}}. \quad (48)$$

For the different classes of models we find the following relations which are evaluated at $r = 3 \times 10^{10}$ cm. For CGW:

$$t_{\text{burst}} = 0.86 \text{ weeks } \alpha_{c,-2}^{0.18} \alpha_h^{-1.1} f_{-1}^{-0.3}, \quad (49)$$

$$t_{\text{store}} = 8.73 \text{ weeks } \alpha_{c,-2}^{-0.49} f_{-1} \dot{M}_{-9}, \quad (50)$$

$$t_{\text{spread}} = 11.1 \text{ yr } \alpha_{c,-2}^{0.21} f_{-1}, \quad (51)$$

and

$$L = 8.49 \times 10^{34} \text{ ergs s}^{-1} \alpha_{c,-2}^{-0.67} \alpha_h^{1.1} f_{-1}^{1.3}. \quad (52)$$

For MM with $\alpha \geq 0.3$:

$$t_{\text{burst}} = 1.29 \text{ weeks } \alpha_c^{0.19} \alpha_h^{-1.1} f_{-0.5}^{-0.3}, \quad (53)$$

$$t_{\text{store}} = 3.70 \text{ weeks } \alpha_c^{-0.5} f_{-0.5} \dot{M}_{-9}^{-1}, \quad (54)$$

$$t_{\text{spread}} = 1.30 \text{ weeks } \alpha_c^{0.21} f_{-0.5}^{-0.42}, \quad (55)$$

and

$$L = 8.42 \times 10^{33} \text{ ergs s}^{-1} \alpha_c^{0.025} \alpha_h^{1.1} f_{-0.5}^{-0.12}. \quad (56)$$

For MM with $\alpha < 0.3$:

$$t_{\text{burst}} = 0.767 \text{ weeks } \alpha_{c,-1}^{0.30} \alpha_h^{-1.1} f_{-0.5}^{-1.1}, \quad (57)$$

$$t_{\text{store}} = 14.8 \text{ weeks } \alpha_{c,-1}^{-0.8} f_{-0.5} \dot{M}_{-9}^{-1}, \quad (58)$$

$$t_{\text{spread}} = 15.0 \text{ weeks } \alpha_{c,-1}^{0.34} f_{-0.5}^{-0.42}, \quad (59)$$

and

$$L = 1.61 \times 10^{35} \text{ ergs s}^{-1} \alpha_{c,-1}^{-1.1} \alpha_h^{1.1} f_{-0.5}^{1.3}, \quad (60)$$

where the subscripts c and h stand for cold and hot (i.e., quiescent and outburst). Here the MM model is also generalized to a 2α -model, although it was originally proposed by MM that α is constant. Note that we have assumed $l^* = 1$, so that $\alpha_{\text{cold}} = 0.3$ divides $\Sigma_{\text{max},1}$ and $\Sigma_{\text{max},2}$.

We see that for the CGW models with a cold torus, the orientation of time scales is $t_{\text{burst}} < t_{\text{store}} < t_{\text{spread}}$, but that for the models based on the partial ionization instability the orientation for all reasonable parameters is $t_{\text{burst}} < t_{\text{spread}} < t_{\text{store}}$. This means that in terms of these idealized time scales t_{store} is to be identified with t_{twixt} , as was done in CGW and Cannizzo, Wheeler, and Ghosh (1983), but that for the MM models one must take $t_{\text{twixt}} = t_{\text{spread}}$. A comparison of these time scales with those of nonthermal equilibrium treatments (Smak 1983a; PFL), however, shows that the burst time (rate of decline of bolometric luminosity, for example) can, in general, be much faster than the simple viscous time used both here and by Mantle and Bath (1983). The controlling time scale is, in fact, the cooling transition front which takes the disk from a high to a low viscosity state. The argument by Mantle and Bath (1983) and Cannizzo, Wheeler, and Ghosh (1983) that $\alpha \approx 1$ in the outburst state also ignores this effect, taking into account only viscous evolution of the disk and not nonthermal equilibrium phase transitions. In addition, our values for t_{spread} appear smaller than those found in other studies because of the neglect of optically thin conditions. Hence, although equations (49)–(60) are useful in setting the general ordering of time scales, they cannot be used to set quantitative limits on the instability mechanisms in the manner attempted by Cannizzo *et al.* With appropriate expressions for t_{burst} and t_{spread} , useful inequalities based on the time scales could still be constructed.

For any model, a sufficient amount of material must be stored in the quiescent state to give a bright burst. The bolometric luminosity can be cast in a form which is independent of the above time scales to use as a check against observed dwarf novae. From standard disk theory the effective temperature in a steady-state disk is obtained by equating σT_{eff}^4 to the surface flux given in equation (7). Because of the correction term $[1 - \beta\sqrt{(r_{\text{wd}}/r)}]$, the quantity T_{eff} peaks at $r = 49/36 r_{\text{wd}}$ for $\beta = 1$. This maximum effective temperature can be written as

$$T_{\text{eff,max}} = 19,900 \text{ K} (M_{\text{wd}}/1 M_{\odot})^{1/4} (\dot{M}/10^{16} \text{ g s}^{-1})^{1/4} \\ \times (r_{\text{wd}}/10^9 \text{ cm})^{-3/4}. \quad (61)$$

The disk luminosity is given by $L_{\text{disk}} = 1/2 GM_{\text{wd}}\dot{M}/r_{\text{wd}}$. (In the outburst disk this relation should not be directly applied because \dot{M} decreases somewhat with r , but we shall ignore this.) Eliminating \dot{M} between these relations gives

$$L_{\text{disk}} = 4.19 \times 10^{35} \text{ ergs s}^{-1} (T_{\text{eff,max}}/10^5 \text{ K})^4 (r_{\text{wd}}/10^9 \text{ cm})^2. \quad (62)$$

It is unfortunate that L_{disk} depends so strongly on an uncertain parameter like $T_{\text{eff,max}}$. SS Cyg is the only system for which a reliable value has been obtained for the outburst disk (Kiplinger 1979; Córdova and Mason 1982). By fitting theoretical disk spectra to observed spectra, a value for $T_{\text{eff,max}}$ of roughly 100,000–150,000 K is obtained. Taking $r_{\text{wd}} = 5 \times 10^8$ cm gives $L_{\text{disk}} \approx 1\text{--}5 \times 10^{35} \text{ ergs s}^{-1}$.

One can get some idea of how the burst luminosities of other dwarf novae systems compare to SS Cyg by comparing their peak visual magnitudes—after correcting for disk inclination and distance. Córdova and Mason (1982) list a total of seven objects classified as dwarf novae for which distances have been measured. These are shown in Table 4. The last column contains the visual luminosity times $d^2/\cos i$, normalized to 1 for SS Cyg. Inasmuch as visual magnitude is proportional to bolometric luminosity, this quantity corresponds to L_{disk} . The luminosities of the last four systems are within a

factor of 2.5 of SS Cyg and hence should also be of order $10^{35} \text{ ergs s}^{-1}$. The first three systems have much smaller luminosities. This is to be expected from the standpoint of a disk instability. Their periods and hence binary separations are smaller, so a smaller amount of material is stored in quiescence.

V. CONCLUSION

This numerical study of thin disk accretion covers the region of parameter space appropriate to dwarf novae and X-ray transients. We have used new opacities to investigate a previously unstudied regime of steady-state models in which the solutions are cool, radiative, and optically thick. A simplified optically thin treatment was used to study solutions at even lower rates of accretion. These solutions are complex and double-valued. We have also shown that for all values of α less than unity the steady-state models are optically thick at Σ_{max} . Thus, the instability cannot recur by increase of surface density without the system becoming optically thick.

A thorough examination of the previously discovered extrema in the loci of steady-state models reveals that two effects induce maxima in surface density: the rapid variation of opacity with temperature at α near unity, and the change in convective efficiency with temperature at lower α . The presence of these two maxima can have several effects. The midplane temperature and molecular weight and hence the viscous time are different for the two maxima. Since the dominant maximum is different for different α , care must be taken to choose conditions self-consistently; i.e., physics based on the opacity peak maximum should not be combined with a choice of α which causes the convective maximum to be dominant. In addition, Mineshige and Osaki (1983) have shown that when both maxima are of roughly equal value, a plateau on the rise to maximum in the theoretical light curves can result, which is not observed. This can be avoided by reducing the mixing length to enhance the opacity peak maximum, or by reducing α to enhance the convective maximum.

The models of steady-state structure we have presented are only a prelude to a complete time-dependent study. These steady-state solutions do provide the locations of the points of instability and can be used to define various time scales of

TABLE 4
RELATIVE PEAK VISUAL LUMINOSITIES^a

DN	P (hr)	$r_{10.5}^b$	V_{peak}	$L_{v,\text{app}}^c$	i^d	$\cos i$	d (pc)	$L_{v,\text{corr}}^e$
OY Car	1.51	0.37	11.7	0.036	78 (± 3)	0.208	150	0.20
EX Hya	1.64	0.39	10.0	0.174	> 70	< 0.342	76–190	0.15–0.96
Z Cha	1.79	0.41	11.9	0.030	79 (± 2)	0.191	125 (± 20)	0.13
U Gem	4.25	0.73	8.8	0.525	67 (± 8)	0.391	76 (± 30)	0.39
SS Cyg	6.60	0.98	8.1	1.000	37 (± 3)	0.799	125 (± 25)	1.00
EM Cyg	6.98	1.02	11.9	0.030	~ 65	0.423	320	0.37
BV Cen	14.63	1.67	10.5	0.110	61 (± 5)	0.485	450	2.40

^aFrom Córdova and Mason 1982.

^bAssuming $P^2(M_1 + M_2) = 4\pi^2 a^3/G$, $M_1 + M_2 = 1 M_{\odot}$, and $r = a/4$.

^cApparent peak visual luminosity, SS Cyg = 1.

^dDisk inclination in degrees.

^ePeak visual luminosity corrected for distance and disk inclination, SS Cyg = 1.

interest. We defer to future papers detailed discussions of the implications of these models for time-dependent behavior.

Our preliminary vertically averaged time-dependent models based on the instability at the point of convective onset give a satisfactory picture of many aspects of the outbursts of dwarf novae and soft X-ray transients (Cannizzo, Wheeler, and Ghosh 1983). A ring formed at the expected radius for dwarf novae, $\sim 3 \times 10^{10}$ cm, containing the amount of matter expected for the convective instability model for $\alpha_{\text{cold}} = 0.01$ gives an appropriate asymmetric burst with a rapid rise and slower decay, with the proper peak magnitude, $\sim 10^{35}$ ergs s^{-1} , to match the observations with α in the hot state of order unity. The same values of α in the hot and cold states and a critical density appropriate to the larger orbit of Aquila X-1 give a reasonable fit to the X-ray and optical outbursts of that classical soft X-ray transient.

The rise to optical maximum in these models occurs as the material spreads out from the original ring on a viscous time scale which is rapid enough, of order 10 hr, to be comparable to the time scale of the thermal instability. This means our approximation of placing the ring in the hot state instantaneously is somewhat crude, and a complete time-dependent study resolving the evolution of the instability on a thermal time scale will be necessary. Nevertheless, the evolution of the continuum from the disk is similar to that observed. There is at first an approximately Planckian spectrum, peaking in the optical, from the hot ring. As the ring spreads into a disk, the peak shifts to the ultraviolet, and in the middle wavelengths the continuum has a $\nu^{1/3}$ slope. The continuum then decays in an approximately self-similar manner as material drains out of the disk. A time-dependent spectral evolution is shown in Figure 15.

As we noted in § IV, these simple models may be in error by neglecting the effects of the cooling transition wave which may speed the evolution of the light curve in the drop from maximum light. This phase is complex and has not yet, in our point of view, been treated with realistic physics.

As the material cools from the point of instability at Σ_{min} , it will tend to become optically thin before reaching steady state at the lower temperature. Williams (1980) and FLP argue that this will cause the emissivity to decrease and the temperature to remain at ~ 6000 K. We have shown here (Fig. 4, and associated discussion) that this tends to happen only at smaller radii and large $\alpha \approx 1$. The critical value of α above which only a warm branch exists is given by $0.1\mu r_{10}^{3/2}$. For the inner regions ($r_{10} < 1$) $\alpha \geq 0.1$ will give only a warm solution, but in material present at larger r the disk will be in a cold state ($T < 2500$ K). For $\alpha \approx 0.1$, as assumed by PFL, the only equilibrium solutions near the injection radius, $\sim 2 \times 10^{10}$ cm, are at low temperature, viz., ~ 2000 K. If α decreases with temperature, this tendency to develop cold solutions in quiescence is enhanced. In such a case, the cold, low-viscosity region should store the injected matter but choke the flow to the inner regions. Any matter which is hung up in an inner warm, optically thin regime should have a higher viscosity and continue to drain onto the central star rather than accumulate matter, as shown by present time-dependent models based on less detailed physics. Such regions could be the origin of the emission lines observed in quiescence, but seem likely not to

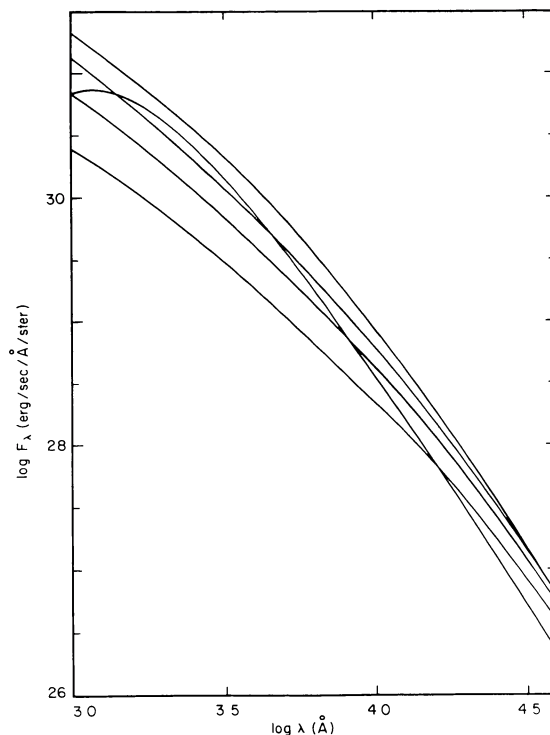


FIG. 15.—Spectral evolution of a hot ring spreading into an outburst disk is shown. Time-dependent method of Bath and Pringle (1981) is used. Initial conditions are $\Sigma_{\text{max}} = 590 \text{ g cm}^{-2}$, $\delta r/r_{\text{ring}} = 0.2$, $r_{\text{ring}} = 3 \times 10^{10}$ cm. We used $\alpha = 1$. Times shown are for $t = 0, 0.05, 0.1, 0.5,$ and 1 week. Curve with the peak at $\lambda \approx 1000 \text{ \AA}$ represents the initial hot ring which radiates like a blackbody at $T_{\text{eff}} \approx 30,000$ K. Disk which is subsequently formed is much hotter ($T_{\text{eff,max}} \approx 100,000\text{--}200,000$ K). As the stored material is cleared out, the power at all frequencies decreases.

represent the bulk of the matter which is too cool to be observed easily.

Our current analysis suggests that the material must turn optically thick before it can undergo an outburst. For any value of α , especially for $\alpha < 0.3$ where $\tau_{\text{mid}} \approx 10^4\text{--}10^6$, we find that the surface density corresponding to optical depth unity is at least a factor of 2 or 3 less than Σ_{max} . From preliminary time-dependent work we find the time scale to augment Σ by this amount in the quiescent ring just before Σ_{crit} is attained is ~ 10 days. Optically thin emission lines are observed, however, up until a few hours before the burst occurs (Hessman 1983). This suggests that the material responsible for the emission lines is not the source of the outburst. If the outburst occurs in cold dense material which is not contributing to the emission lines, then the lines could be emitted by the dilute warm inner material right up to the point of outburst.

Finally, the relatively large optical depths which we find in this study also have consequences for the model of dwarf nova eruptions induced by variations in the mass transfer rate from the secondary (Bath and Pringle 1981; Mantle and Bath 1983). In particular, since no optically thick disk is observed in quiescence (Kiplinger 1979), the rate of accretion in the disk must be small. One can then ask at what rate of accretion the

inner edge of the disk turns optically thin. A typical white dwarf radius is 5×10^8 cm, so that our solutions near 3×10^9 cm are approximately representative. These solutions are optically thick for accretion rates as low as $10^{-13} M_{\odot} \text{ yr}^{-1}$. The quiescent value of the mass transfer rate adopted in the studies of mass transfer variation is $\sim 10^{-9} M_{\odot} \text{ yr}^{-1}$. Such rates would seem to demand optically thick disks in quiescence, in contradiction to the observations.

We gratefully acknowledge useful conversations with Joe Smak, Doug Lin, John Faulkner, Rob Robinson, Ed Nather, Bohdan Paczyński, Ron Webbink, Jim Truran, Sumner Starrfield, Bob Williams, Hideyuki Saio, Hollis Johnson, and Frederic Hessman. This research was supported in part by grants from the R. A. Welch Foundation and from NASA grant NSG 7232.

REFERENCES

- Alexander, D. R., Johnson, H. R., and Rypma, R. L. 1983, *Ap. J.*, **272**, 773.
 Alme, M. L., and Wilson, J. R. 1973, *Ap. J.*, **186**, 1015.
 Auman, J. R. 1966, *Ap. J. Suppl.*, **14**, 171.
 Bath, G. T., and Pringle, J. E. 1981, *M.N.R.A.S.*, **194**, 967.
 ———. 1982, *M.N.R.A.S.*, **199**, 267.
 Böhm-Vitense, E. 1958, *Z. Ap.*, **46**, 108.
 Cannizzo, J. K. 1981, M.A. thesis, University of Texas at Austin.
 Cannizzo, J. K., Ghosh, P., and Wheeler, J. C. 1982, *Ap. J. (Letters)*, **260**, L83.
 Cannizzo, J. K., Wheeler, J. C., and Ghosh, P. 1982, in *Pulsations in Classical and Cataclysmic Variable Stars*, ed. J. P. Cox and C. J. Hansen (Boulder: University of Colorado Press), p. 13.
 ———. 1983, in *Proc. Cambridge Workshop on Cataclysmic Variables and Low-Mass X-Ray Binaries* (Dordrecht: Reidel), in press.
 Chevalier, R. A. 1981, *Fund. Cosmic Phys.*, **7**, 1.
 Chitre, S. M., and Shaviv, G. 1967, *Proc. Nat. Acad. Sci.*, **57**, 573.
 Córdova, F. A., and Mason, K. O. 1982, *Accretion Driven Stellar X-Ray Sources* (Cambridge: Cambridge University Press).
 Cox, A. N., and Stewart, J. N. 1969, *Sci. Inf., Astr. Council, Acad. Sci. USSR*, **No. 15**, p. 1.
 Faulkner, J., Lin, D. N. C., and Papaloizou, J. 1983, *M.N.R.A.S.*, **205**, 359.
 Hensler, G. 1982a, *Astr. Ap.*, **114**, 309.
 ———. 1982b, *Astr. Ap.*, **114**, 319.
 Hessman, F. V. 1983, private communication.
 Hoshi, R. 1979, *Progr. Theor. Phys.*, **61**, 1307.
 ———. 1981, *Progr. Theor. Phys. Suppl.*, **70**, 181.
 ———. 1982, *Progr. Theor. Phys.*, **67**, 179.
 Iben, I., Jr. 1963, *Ap. J.*, **138**, 452.
 Joss, P. C., Salpeter, E. E., and Ostriker, J. P. 1973, *Ap. J.*, **181**, 429.
 Kiplinger, A. L. 1979, *Ap. J.*, **234**, 997.
 Kippenhahn, R., and Thomas, H.-C. 1982, *Astr. Ap.*, **114**, 77.
 Kippenhahn, R., Weigert, A., and Hofmeister, E. 1967, in *Methods in Computational Physics*, ed. B. Alder, S. Fernbach, and M. Rotenberg (New York: Academic), p. 129.
 Koen, M. C. 1976, M.A. thesis, University of Capetown.
 Kozłowski, M., Wiita, P. J., and Paczyński, B. 1979, *Acta Astr.*, **29**, 157.
 Lightman, A. P., and Eardley, D. M. 1974, *Ap. J. (Letters)*, **187**, L1.
 Lin, D. N. C., and Papaloizou, J. 1980, *M.N.R.A.S.*, **191**, 37.
 Mantle, V. J., and Bath, G. T. 1983, *M.N.R.A.S.*, **202**, 151.
 Meyer, F., and Meyer-Hofmeister, E. 1981, *Astr. Ap.*, **104**, L10.
 ———. 1982, *Astr. Ap.*, **106**, 34.
 ———. 1984, *Astr. Ap.*, in press.
 Mineshige, S., and Osaki, Y. 1983, *Pub. Astr. Soc. Japan*, **35**, 377.
 Novikov, I. D., and Thorne, K. S. 1973, in *Black Holes* (New York: Gordon & Breach), p. 343.
 Osaki, Y. 1974, *Pub. Astr. Soc. Japan*, **26**, 429.
 Papaloizou, J., Faulkner, J., and Lin, D. N. C. 1983, *M.N.R.A.S.*, **205**, 487.
 Piran, T. 1978, *Ap. J.*, **221**, 652.
 Pringle, J. E. 1981, *Ann. Rev. Astr. Ap.*, **19**, 137.
 Robertson, J. A., and Tayler, R. J. 1981, *M.N.R.A.S.*, **196**, 185.
 Robinson, E. L. 1976, *Ann. Rev. Astr. Ap.*, **14**, 119.
 Schwarzschild, M. 1958, *Structure and Evolution of the Stars* (New York: Dover).
 Shakura, N. I., and Sunyaev, R. A. 1973, *Astr. Ap.*, **24**, 337.
 ———. 1976, *M.N.R.A.S.*, **175**, 613.
 Smak, J. 1971, in *IAU Colloquium 15, New Directions and New Frontiers in Variable Star Research*, ed. W. Strohmeyer (Bamberg: Veröff. Remeis-Sternw.), p. 248.
 Smak, J. 1976, *Acta Astr.*, **26**, 277.
 ———. 1982a, *Acta Astr.*, **32**, 199.
 ———. 1982b, *Acta Astr.*, **32**, 213.
 ———. 1983a, *Ap. J.*, **272**, 234.
 ———. 1983b, *Acta Astr.*, **33**, 333.
 ———. 1984, *Ap. J.*, in press.
 Tayler, R. J. 1980, *M.N.R.A.S.*, **191**, 135.
 Tylenda, R. 1981, *Acta Astr.*, **31**, 127.
 Vila, S. C. 1978, *Ap. J.*, **223**, 979.
 ———. 1980, *Ap. J.*, **241**, 355.
 Williams, R. E. 1980, *Ap. J.*, **235**, 939.

JOHN K. CANNIZZO and J. CRAIG WHEELER: Department of Astronomy, University of Texas, Austin, TX 78712